Are Large Sulfur Isotope Variations Biosignatures in an Ancient, Impact-Induced Hydrothermal Mars Analog?

Christopher J. Tino[1]*, Eva E. Stüeken[2,3], Gernot Arp[4], Michael Ernst Böttcher[5,6,7], Steven M. Bates[1], Timothy W. Lyons[1,3]

1. Department of Earth and Planetary Sciences, University of California, Riverside CA 92521, USA
2. School of Earth and Environmental Sciences, University of St. Andrews, St. Andrews, Fife, KY16 9AL, Scotland, UK
3. Virtual Planetary Laboratory, University of Washington, Seattle WA 98195, USA
4. Georg-August-Universität Göttingen, Geowissenschaftliches Zentrum, Goldschmidtstrasse 3, 37077 Göttingen, Germany
5. Geochemistry & Isotope Biogeochemistry, Leibniz Institute for Baltic Sea Research (IOW), Seestrasse 15, D-18119 Warnemünde, Germany
6. Marine Geochemistry, University of Greifswald, Friedrich-Ludwig-Jahn Str. 17a, D-17489 Greifswald, Germany
7. Department of Maritime Systems, Interdisciplinary Faculty (INF), University of Rostock, Albert-Einstein-Straße 21, D-18059 Rostock, Germany
*Corresponding author: ctino001@ucr.edu

Abstract

Discrepancies have emerged concerning the application of sulfur stable isotope ratios as a biosignature in impact crater paleolakes. The first in-situ $\delta^{34}S$ data from Mars at Gale crater display a ~75‰ range that has been attributed to an abiotic mechanism. Yet biogeochemical studies of ancient environments on Earth generally interpret $\delta^{34}S$ fractionations > 21‰ as indicative of a biological origin, and studies of $\delta^{34}S$ at analog impact crater lakes on Earth have followed the same approach. We performed analyses (including $\delta^{34}S$, TOC wt%, and SEM imaging) on multiple lithologies from the Nördlinger Ries impact crater, focusing on hydrothermally altered impact breccias and associated sedimentary lake-fill sequences to determine whether the $\delta^{34}S$ properties define a biosignature. The differences in $\delta^{34}S$ between the host lithologies may have resulted from thermochemical sulfate reduction, microbial sulfate reduction, hydrothermal equilibrium fractionation, or any combination thereof. Despite abundant samples and instrumental precision currently exclusive to Earth-bound analyses, assertions of biogenicity from $\delta^{34}S$ variations > 21‰ at the Miocene Ries impact crater are tenuous. This discourages the use of $\delta^{34}S$ as a biosignature in similar environments without independent checks that include the full geologic, biogeochemical, and textural context, as well as a comprehensive acknowledgment of alternative hypotheses.

1. Introduction

Impact crater lakes may have housed the earliest (> 3.5Ga) habitable environments on Earth and Mars. In these locations, impact-induced hydrothermal activity would have provided heat in opposition to a faint young Sun and could have sourced compounds thought necessary for prebiotic synthesis of life's building blocks as well as the bioessential elements needed to sustain life (Abramov and Kring, 2005; Cockell *et al.*, 2020; Farmer, 2000; Kacar *et al.*, 2020; Kring, 2000; Osinski *et al.*, 2013). These attributes make impact craters appealing targets for origin-of-life studies and the search for extinct life on Mars. In fact, impact craters have been the sites of multiple surface exploration missions, including the landing of the Perseverance rover in Jezero crater (Goudge *et al.*, 2015; Grotzinger *et al.*, 2015; Osinski *et al.*, 2020; Mangold *et al.*, 2021).

The collective understanding of nutrient cycling in ancient crater lakes has long relied on studies of geochemical proxies at well-preserved analog environments on Earth's surface (Hays *et al.*, 2017; Léveillé, 2010; Osinski *et al.*, 2020). One such proxy is the ratio of the two most abundant stable isotopes of sulfur (*i.e.*, $\delta^{34}S = [(^{34}S/^{32}S)_{sample}/(^{34}S/^{32}S)_{Vienna\text{-}Canyon\ Diablo\ Troilite} - 1] \times 1000$), which has the potential to illuminate both internal and surface processes on Earth and Mars (Nielsen *et al.*, 1991; Canfield, 2001; Franz *et al.*, 2019; King and McLennan, 2010). Sulfur has an expanded valence octet that allows for a redox continuum, with oxidation states ranging from -2 to +6. Stable S-isotope ratios can be fractionated during chemical exchanges across this range by kinetic and equilibrium reactions linked to both abiotic and biological processes (Canfield, 2001; Baune and Böttcher, 2010; Sakai, 1957; Seal, 2006; Surkov *et al.*, 2012; Thode *et al.*, 1961).

Mars can be considered a S-rich planet, evidently possessing a higher relative surface abundance of S than present-day Earth (Clark *et al.*, 1982; Franz *et al.*, 2019). Sulfur has been examined on the Martian surface in a multitude of forms, including Fe-sulfides (*e.g.*, pyrrhotite [$Fe_{1-x}S$] and pyrite [FeS_2]); Ca/ Mg/Fe-sulfates, such as anhydrite [$CaSO_4$]; and the Fe-hydroxide-sulfate mineral jarosite [$KFe_3(SO_4)_2(OH)_6$] (Franz *et al.*, 2019; Squyres *et al.*, 2004; Vaniman *et al.*, 2014). The reference base of the stable S-isotope system, Vienna-Canyon Diablo Troilite ([VCDT]: $\delta^{34}S$ = 0‰, $^{34}S/^{32}S = 441.626 \pm 0.039 \times 10^{-4}$; Ding *et al.*, 2001), presents a practical comparative scale for both Mars and Earth, because it reflects the S isotope composition of our

solar system's primordial terrestrial material (Hoefs, 2021; Sharp, 2017; Thode *et al.*, 1961). Sulfur isotope ratios in Martian crater settings therefore have great potential to provide novel insights into past environmental conditions, including the presence of life. However, before this geochemical signature can be applied as a potential proxy for biological activity, it is imperative to develop a more thorough understanding of the range of possible S-isotope-fractionating processes that can operate in impact craters.

The complexity surrounding S fractionation mechanisms has provided the basis of multiple recent studies investigating S cycling in ancient impact craters (*e.g.*, Kring *et al.*, 2021; Schaefer *et al.*, 2020, 2022). Hydrothermal mineral assemblages from borehole samples of Chicxulub crater's peak rim display anhydrite and pyrite with $\Delta^{34}S_{sulfate\text{-}sulfide}$ values of 25‰ to 54‰ (Kring *et al.*, 2021). There, consistent visual evidence of pyrite framboids bolsters an interpretation of microbial sulfate reduction [MSR] as the primary fractionation mechanism (Kring *et al.*, 2021). At Haughton crater in the Canadian High Arctic, a $\Delta^{34}S_{sulfate\text{-}sulfide}$ of 44‰ was observed between gypsum and pyrite, along with a $\Delta^{34}S_{sulfate\text{-}sulfide}$ of 71‰ between gypsum and marcasite [orthorhombic FeS_2]. Due to the magnitude of these differences, these data have also been interpreted as MSR (Parnell *et al.*, 2010). However, there is a lack of reported sedimentary framboidal pyrite, the formation of which is often attributed to high rates of dissimilatory sulfate reduction associated with organic matter degradation (Passier *et al.*, 1999; Rickard, 2021). This form notably differs from euhedral pyrite, which can form in sediments via lower microbial process rates, overgrowths on framboids (Passier *et al.*, 1999), recrystallization (Liaghati *et al.*, 2005), or a combination thereof. *In situ* analyses of S isotopes have been made by the Mars Science Laboratory's [MSL] Sample Analysis at Mars [SAM] instrument suite at Gale crater (Franz *et al.*, 2017). The reported values span from -47 (± 14)‰ to 28 (± 7)‰, which is noted as similar to the terrestrial range observed on Earth (Franz *et al.*, 2017; Hoefs, 2021). A multi-step abiotic fractionation mechanism was proposed, which included atmospheric oxidation and ultraviolet photolysis of volcanogenic S, followed by hydrothermal equilibrium fractionation (Franz *et al.*, 2017). These contradictory interpretations—specifically, thermophilic MSR at impact craters on Earth versus a set of abiotic reactions for the first *in situ* surface $\delta^{34}S$ analyses from Mars—call for additional understanding of sulfur isotope ratios and related controls at analog sites.

To shed further light on these contrasting studies and their respective implications, we have performed a study of multi-phase sulfur speciation and isotope partitioning at the Ries crater in southern Germany. Our aim is to determine if and when large S isotope fractionation events in crater lake systems are definitively linked to life. Accordingly, we explore the three plausible mechanisms known to produce significant $\delta^{34}S$ variation in crater settings: MSR, thermochemical sulfate reduction [TSR], and hydrothermal equilibrium fractionation.

2. Geologic Setting

The Nördlinger Ries, located 110 km northwest of Munich, Germany, is one of the best-studied craters on Earth (**Fig. 1**) (Arp *et al.*, 2013a; Graup, 1999; Newsom *et al.*, 1990; Pohl *et al.*, 1977; Stöffler *et al.*, 2013). It is ~24 km in diameter and was generated at 14.7495 ± 0.016 Ma by the impact of a 1.3 ± 0.2 km-diameter meteorite (Artemieva *et al.*, 2013; Di Vincenzo, 2022). The target rocks included Mesozoic sedimentary strata and Variscan crystalline basement rocks (Pohl *et al.*, 1977; Stöffler *et al.*, 2013; Sturm *et al.*, 2013). The Ries crater is the type locality for suevite, an impact melt-bearing breccia now identified at several terrestrial crater sites where crystalline rocks compose all or part of the surface target (Osinski *et al.*, 2016; Stöffler *et al.*, 2013). It is considered a Mars analog because—like many craters on Mars—it possesses a well-preserved

dual-layer ejecta [DLE] blanket with a rampart structure (Barlow, 2005; Hörz *et al.*, 1983; Kenkmann and Schönian, 2006; Pohl *et al.*, 1977; Sturm *et al.*, 2013; Viola *et al.*, 2017). The lower ejecta layer is a continuous mixture of sedimentary and crystalline basement rocks termed "Bunte Breccia" (Hörz *et al.*, 1983; Pohl *et al.*, 1977). The upper ejecta layer ["outer suevite"] comprises discontinuous patches of suevite, and suevite also occurs within the central crater basin as a continuous breccia lens ["crater suevite"] (Pohl *et al.*, 1977; Stöffler *et al.*, 2013; von Engelhardt, 1990; von Engelhardt, 1997). Comprehensive reviews of crater formation mechanisms can be found in Artemieva *et al.* (2013) and Stöffler *et al.* (2013). Of direct astrobiological interest is the impact-induced formation of a hydrothermal crater lake system that consequentially interacted with the DLE for roughly 10^4 to 10^6 years (Arp *et al.*, 2013b; Caudill *et al.*, 2021; Muttik *et al.*, 2010; Newsom *et al.*, 1986; Osinksi, 2005; Sapers *et al.*, 2017).

2.1. The Ries Crater Paleolake

A closed-basin lake formed in the Ries basin shortly after the impact and existed for 1–2 Myr (Arp *et al.*, 2021a; Füchtbauer *et al.*, 1977; Jankowski, 1977; Montano *et al.*, 2021). Successive weathering of suevite followed by Bunte Breccia, in combination with diminishing hydrothermal activity, caused multiple distinct shifts in the lake's chemistry through time (Arp *et al.*, 2013a). These shifts correlate approximately with the four stratigraphic units established by Füchtbauer *et al.* (1977) (**Fig. 2**). The first waters in the basin were transient playas that deposited sandstones and reworked suevite, which are now referred to as the basal member or unit A (Füchtbauer *et al.*, 1977). This interval was followed by the formation of a permanent, eutrophic, high-pH alkali-saline lake that deposited the bituminous shales and laminated marls of the organic-rich laminite member (unit B) (Füchtbauer *et al.*, 1977; Arp *et al.*, 2013a; Rullkötter *et al.*, 1990; Stüeken, Tino *et al.*, 2020). Changes in the dominant weathering and alteration source from suevite to Bunte Breccia led to a shift toward saline waters with circum-neutral pH and deposition of calcareous claystones of the marl member (unit C) (Arp *et al.*, 2013a). Then, a change to alternating hyposaline and hypersaline conditions led to deposition of the clay member (unit D) (Arp, 2006; Arp *et al.*, 2013a; Füchtbauer *et al.*, 1977). The youngest preserved lake sediments still show evidence of hydrologically closed conditions with no evidence for an outlet (Arp *et al.*, 2017). Eventually, the lake basin filled with sediment, and lake waters permanently disappeared.

2.2. Impact-induced Hydrothermal Activity

Hydrothermal alteration was pervasive within the central basin, as indicated by the complete replacement of impact-generated glasses in crater suevite (Osinski, 2005; Stöffler, 1977). Melt-rich layers within suevite sequences from multiple drill cores point to temperatures of ~600°C for the first post-impact materials that settled in the basin (von Engelhardt, 1990). The earliest sustained hydrothermal fluids were likely derived from surface meteoric waters and groundwaters from the surrounding country rock. These fluids ranged from 200–300°C as indicated by K-metasomatism and chloritization in crater suevite (Osinski, 2005; Osinski *et al.*, 2004). The second or main stage of alteration occurred via weakly alkaline fluids as temperatures decreased through the 200–100°C window and was characterized by intermediate argillic alteration and zeolitization products within crater suevite (Osinski, 2005). Muttik *et al.* (2010) used stable oxygen [$\delta^{18}O$] and hydrogen [δD] isotope data from crater suevite to constrain the temperatures of the final alteration stage to 43–112°C. Temperature increased monotonously with depth in association with convective circulation, and the coolest stage was likely the longest-lived (Muttik *et al.*, 2010). Quantitative constraints on the duration and intensity of hydrothermal activity as it relates to the paleolake waters are presently limited. Stratigraphically, hydrothermal activity occurred throughout the basal member and extended into the laminite member (Arp *et al.* 2013b). During

deposition of the laminite member, Ca-bearing fluids of both hydrothermal and non-hydrothermal origin were locally introduced to alkaline waters, leading to the formation of carbonate spring mounds and travertines (Arp, 1995; Arp *et al.*, 2013b). The observation of streamer carbonates in the Erbisberg spring mound (coordinates: 48°49′52.34″N, 10°30′42.56″E) indicate that 70°C waters were still emerging from the system several 100 kyr after impact and that hydrothermal effects extended at least to the crater's inner ring (Arp *et al.*, 2013b). While the subsurface impact breccias faced significant exposure to hydrothermal fluid temperatures above the current known limits of life (~121°C), there is no reason to assume that the earliest lake waters, or the sediments deposited from them, ever existed at uninhabitably high temperatures. Such high temperatures would require elevated pressure to maintain water in a liquid state, which is not plausible for this lake system in the Miocene. Given the lateral and vertical extent of hydrothermal activity, drill cores and field sites are highly complementary at Ries crater. This study therefore includes samples from both.

3. Samples and Methods

3.1. Sample Collection

We analyzed the research drill core Nördlingen 1973 [FBN 73], which contains one of the most extensive paleolake sedimentary sections among the Ries drill cores and has been the subject of multiple geochemical studies, which provide valuable context for our $\delta^{34}S$ work (Füchtbauer *et al.*, 1977; Muttik *et al.*, 2010, 2011; Osinski, 2005; Stüeken, Tino *et al.*, 2020; von Engelhardt, 1997). For our examination of the paleolake sediments, 81 samples were selected across 241 m of stratigraphy (**Fig. 2**; 21–262 m depth in the core or 403–164 m above modern sea level [a.s.l.]). To demonstrate that the paleolacustrine $\delta^{34}S$ data collected from the FBN 73 drill core are representative for the whole basin, 27 samples from four exploratory Nördlinger Ries [NR] wells were included (**Fig. 3**; NR-10, NR-20, NR-30, and NR-40 drilled by BEB Erdgas und Erdöl GmbH in the early 1980s; permission for use was provided by ExxonMobil; Rullkötter *et al.*, 1990; Barakat *et al.*, 2012; Barakat *et al.*, 2013). All lacustrine sediment samples in this study have undergone minimal post-depositional geothermal heating. Vitrinite reflectance data from FBN 73 samples suggest a maximum temperature of 60°C (Wolf, 1977). Subsequent biomarker studies of NR cores pointed similarly to very minor thermal overprints (Barakat and Rullkötter, 1995).

We assessed the S chemistry resulting from hydrothermal alteration within the impact breccia by selecting 33 samples spanning 71 m of stratigraphy (**Fig. 2**; 29–100 m core depth, 315–386 m a.s.l.) from the Enkingen [SUBO 18] core. SUBO 18 contains 21 meters of lacustrine sedimentary rock overlying ~65 m of crater suevite, followed by ~15 m of impact melt breccia (*i.e.*, melt content > 50%). This is the only coherent sequence of impact melt breccia encountered in a Ries crater drill core thus far (Pohl *et al.*, 2010; Reimold *et al.*, 2012; Reimold *et al.*, 2013).

Field sampling was included to complement the drill core analyses, with the hope of elucidating the S composition of both the water column of the alkaline lake and the subaerial weathering environment that fed into the basin at that time. Eight samples were collected from two carbonate mounds—Wallerstein travertine (n = 2, 48°53′20.3″N, 10°28′28.9″E) and Goldberg spring mound (n = 6, 48°51′40.7″N, 10°25′19.8″E)—for analysis of carbonate-associated sulfate [CAS] content as a proxy for the SO_4^{2-} composition of the water column during the alkaline lake phase (**Fig. 4**). The Wallerstein samples are from the base of that mound, which is composed of non-fossiliferous carbonates with intercalations of brine shrimp fecal pellets (Pache *et al.*, 2001), signifying that they were deposited synchronously to the pellet-rich lower part of the laminite member (Jankowski, 1977) and formed before the Goldberg mound samples. The sampled portions

of the Goldberg and Wallerstein mounds in this study were formed subaqueously (*i.e.*, in a mixing zone of sub-lacustrine spring and alkaline lake water; Arp, 1995; Pache *et al.*, 2001). Multi-isotope ($^{87}Sr/^{86}Sr$, $\delta^{13}C$, $\delta^{18}O$) constraints on mixing ratios at Ries spring precipitation zones suggest that the majority of SO_4^{2-} available for incorporation as CAS was derived from the lake water (Pache *et al.*, 2001). To evaluate possible S contributions to the inner basin from the surficial weathering of outer suevite, three samples of outer suevite were collected from Riedweg (n = 1, 48°54′54.4″N, 10°26′39.8″E) and Otting (n = 2, 48°52′24.1″N, 10°47′55.0″E).

3.2. Geochemical Analyses

The outer rims of all drill core and field samples were trimmed with either a rock saw or manually operated rock chipper, depending on sample hardness. The resulting interiors were hammered into subcentimeter-sized chips, rinsed with deionized H_2O, and dehydrated at 50°C for a minimum of 48 hours. The rock chips were then pulverized in a ball mill.

Total organic carbon [TOC], total inorganic carbon [TIC], total sulfur [TS], chromium-reducible sulfide [CRS], and CAS data for all FBN 73, SUBO 18, and field samples were collected in the Lyons Biogeochemistry Laboratory at the University of California, Riverside [UCR]. Total Carbon [TC], TIC, and TS were measured via combustion on an Eltra CS-500 carbon-sulfur analyzer, all with precision better than ±0.1 wt%. TOC was then calculated as the difference between measured TC and TIC.

The chromium reduction method (*e.g.*, Canfield *et al.*, 1986) was used to assess S present in sulfide minerals. Specifically, bulk sample powders were mixed with a 1 M $CrCl_2$ (acidified to 0.5 M HCl) solution under a stream of N_2 gas (*i.e.*, anoxic conditions) and brought to a boil to evolve hydrogen sulfide [H_2S] from present CRS phases. That H_2S was trapped in a silver nitrate solution as silver sulfide [Ag_2S], which was then quantified gravimetrically and converted to wt% CRS in the sample, assuming all H_2S precipitated as Ag_2S. For carbonate-rich samples (TIC wt% > 11), powders were decarbonated with 1N HCl prior to chromium reduction. In studies of ancient sediments, CRS is typically dominated by sulfur hosted in pyrite. Consistent with these past studies, previously published petrographic analyses of SUBO 18 confirm pyrite as the predominant S phase in the Ries impact breccia (Reimold *et al.*, 2012; Reimold *et al.*, 2013). Standard deviations [σ] for CRS wt%, as measured from repeat (n = 6) analyses of a randomly selected SUBO 18 sample and repeat analyses (n = 7) of a randomly selected FBN 73 sample, were σ = 0.03 wt% and σ = 0.07 wt%, respectively. Sulfur isotope ratio ($\delta^{34}S$) measurements of those same sets showed σ = 0.23‰ (FBN 73) and σ = 0.16‰ (SUBO 18).

To extract CAS, carbonate samples were rinsed in a 5% NaCl solution for three consecutive nights (the solution being refreshed each day) to remove all easily soluble sulfates. This step was followed by two consecutive deionized H_2O rinses of 24 hours each. To remove organic-S and trace sulfides, the samples were then treated with a 30% H_2O_2 solution, the volume of which was calculated to be ~100x in excess of the organic content as inferred from TOC wt% measurements (assuming a simplified CH_2O stoichiometry). This step was followed by two rinses with deionized H_2O of 24 hours each. The purified carbonates were then acidified with a 4N HCl solution with 5 wt% stannous chloride [$SnCl_2$] until effervescence ceased. Insoluble materials were removed by filtration, followed by addition of a saturated barium chloride [$BaCl_2$] solution to quantitatively precipitate the SO_4^{2-} as $BaSO_4$. The volume of added $BaCl_2$ was calculated to be roughly 40x in excess of the CAS as estimated by conservatively assuming that the measured wt% TS was entirely CAS. CAS concentrations (mg/kg) were then calculated via gravimetry of the filtered and dried $BaSO_4$. Triplicate analyses of a randomly selected carbonate sample yielded a coefficient of

variation [CV; ratio of σ to the mean] = 0.1% for CAS contents, and $\delta^{34}S$ values for that same triplicate agreed to within 0.1‰.

Sulfur isotope ratios for the CRS and CAS were measured at UCR using a Thermo Scientific Delta V Plus continuous-flow stable isotope ratio mass spectrometer [IRMS]. Sulfur from Ag_2S and $BaSO_4$ was converted to SO_2 and separated via gas chromatography [GC] on a Costech ECS 4010, with gas flow to the IRMS controlled by a Thermo Scientific ConFlo III open split interface. For $\delta^{34}S_{CRS}$, samples were bracketed by the international reference standards IAEA-S1, -S2, and -S3. For $\delta^{34}S_{CAS}$, samples were bracketed by IAEA-SO5, -SO6, and NBS-127 (for the $\delta^{34}S$ values of these standards, see Appendix 1 of Sharp, 2017). Precision for all standards in all runs was better than σ = 0.3‰.

Bulk sediment (*i.e.*, including all S in a given sample) and kerogen enrichments of NR-10, NR-20, NR-30, and NR-40 were analyzed at ICBM Oldenburg for TC and TS using a Carlo Erba EA 1108 elemental analyzer. Carbonate was removed with dilute HCl, and TOC was determined coulometrically using a Ströhlein-type 702 Coulomat. TIC contents were obtained from the difference between TC and TOC. The kerogen fraction was separated as described in Barakat and Rullkötter (1995), where solvent-extracted residues are demineralized with a HF:HCl (1:1) treatment followed by additional Soxhlet and ultrasonic extractions. Bulk sediment and kerogen samples were analyzed for $\delta^{34}S$ using combustion-isotope-ratio-monitoring mass spectrometry [C-irmMS]—specifically, a Finnigan MAT 252 mass spectrometer coupled to a Carlo Erba EA 1108 elemental analyzer via a Finnigan MAT ConFlo II open split interface, as described in detail by Böttcher *et al.* (1998) and Böttcher and Schnetger (2004). IAEA-S1, -S2, and -S3, as well as NBS 127, were used to calibrate the $\delta^{34}S$ values to VCDT. Precision for the measurements was better than σ = 0.2‰. Isotope values reported in "‰" are equivalent to "mUr" (milli-Urey; Brand and Coplen, 2012).

Backscattered electron [BSE] imaging (**Fig. 6**) was performed in the Brounce Geochemistry Laboratory at UCR using a JEOL JCM-7000 benchtop scanning electron microscope [SEM]. A combination of manual observations and montage imaging was used to examine the entirety of polished surfaces.

4. Results

4.1. Paleolake Sediments

4.1.1. FBN 73

Starting from the lowest sample depth (261.5 m), $\delta^{34}S_{CRS}$ values of sedimentary rocks from FBN 73 (**Fig. 2, Supplemental Table 1**) are uniformly negative in the basal member (mean = -9.9‰, n = 3, σ = 6.5‰, 261. 5 m - 258.5 m). Moving upcore into the laminite member, values shift from -19.0‰ at 258.5 m to 28.1‰ at 254.5 m, and reach a maximum of 45.1‰ at 237.5 m within an interval characterized by high values (mean = 38.0‰, n = 19, σ = 4.6‰) spanning from 248.5 m to 206.5 m. Values generally decrease over the remainder of the laminite member, with the unit reaching its minimum of 17.5‰ just before the transition into the marl member at 145 m depth. This trend of decreasing values continues throughout the marl (mean = 6.9‰, n = 23, σ = 8.3‰, 140.5 m - 52.1 m) and clay (mean = -1.2‰, n = 10, σ = 13.5‰, 49.1 m - 21.55 m) members but the data have a larger spread.

CRS contents (dominantly pyrite; see Samples and Methods) vary from 0.02 wt% to 5.65 wt%. Values throughout the entire laminite member (mean = 0.30 wt%, n = 48, σ = 0.27 wt%) are generally lower than those within the other units (basal member [mean = 1.35 wt%, n = 3, σ = 0.09 wt%], marl member [mean = 1.09 wt%, n = 23, σ = 0.67 wt%], and clay member [mean = 2.77

wt%, n = 10, σ = 1.57 wt%]). Coefficients of determination [R^2] via linear regression show weak or no relationship between CRS wt% and $\delta^{34}S_{CRS}$ ($R^2 = 0.15$ for all samples, and $R^2 \leq 0.35$ in all individual stratigraphic units). TOC contents follow the trends reported in Förstner (1977) and Stüeken, Tino *et al.* (2020). The basal, laminite, and marl members display no discernable relationship between wt% CRS and TOC ($R^2 < 0.04$ in all cases), but the clay member shows a positive relationship with an R^2 of 0.79.

4.1.2. NR-10, NR-20, NR-30, and NR-40

Data from the four exploratory wells (**Fig. 3**, **Supplemental Table 2**) allow for a wider breadth of $\delta^{34}S$ examination in terms of both sedimentary host phases and spatial distributions within the lake basin. Bulk and kerogen $\delta^{34}S$ data ($\delta^{34}S_{Bulk}$ and $\delta^{34}S_{Kerogen}$) show trends that are similar, in both magnitude and pattern, to the $\delta^{34}S_{CRS}$ values from FBN 73. For any given sample where both $\delta^{34}S_{Bulk}$ and $\delta^{34}S_{Kerogen}$ were measured (n = 3), the differences were minor (≤ 0.5‰) between the two measured phases. Viewed within this context, our bulk measurements indicate that $\delta^{34}S$ is uniformly elevated in the lower laminite member, regardless of which S-bearing phase dominates the isotopic mass balance (*e.g.*, kerogen or pyrite) within a given sample. Moving up core, the combined data series rises from a minimum $\delta^{34}S_{Bulk}$ of 7.4‰ to a maximum $\delta^{34}S_{Bulk}$ of 44.2‰. There is a consistent up-core decrease over the remainder of the sample set, with data from the four uppermost adjusted sample depths (using NR-30 as a zero-reference line) falling below 15‰ (mean = 12.65‰, n = 4, 100.0 m - 51.5 m).

4.1.3. Carbonate Mounds

$\delta^{34}S_{CAS}$ values of the carbonates (**Fig. 4, Supplemental Table 3**) show a range from 26.4‰ to 44.5‰ (mean = 32.1‰, n = 8, σ = 5.5‰). Analyses from Wallerstein travertine ($\delta^{34}S_{CAS}$ = 36.3‰, 44.5‰) display higher values than those from the Goldberg spring mound (mean = 29.3‰, n = 6, σ = 1.8‰). CAS contents range from 1075 mg/kg to 4091 mg/kg, and there is strong negative correlation between CAS content and $\delta^{34}S_{CAS}$, where samples with lower CAS contents tend to have higher $\delta^{34}S_{CAS}$ ($R^2 = 0.81$). TIC for all carbonate samples is 11.6 wt% or greater (compared to 12 wt% for pure $CaCO_3$), attesting to their very low insoluble, siliciclastic contents. CRS contents were 30 mg/kg or lower and represent ≤ 5% of the measured TS in any given sample, suggesting that the risk of isotopic contamination from CRS oxidation during CAS extraction is low.

4.2. Impact Breccias

4.2.1. SUBO 18 (Crater Suevite)

The lowest sample depths (99.35 m - 86.4 m) of SUBO 18 are composed of impact melt breccia (n = 13) and have $\delta^{34}S_{CRS}$ values that generally decrease up core, ranging from 9.1‰ to -19.0‰ (**Fig. 2, Supplemental Table 1**). The transition into crater suevite at 82.92 m coincides with a continued decrease until the minimum of -31.4‰ is reached at 68.59 m depth. This minimum is 4.5‰ lower than the next lightest value (-26.9‰ at 78.23 m) and does not appear to be representative of crater suevite (mean: -20.2‰, n = 20, σ = 5.8‰) or the entire set of impact breccia samples (mean: -15.8‰, n = 33, σ = 9.1‰). $\delta^{34}S_{CRS}$ then increases monotonically over the remainder of the core, reaching the crater suevite maximum of -7.1‰ at 30.73 m, near the top of the analyzed interval. CRS wt% spans from 0.04% to 2.57% and differs in its relationship with $\delta^{34}S_{CRS}$ depending on rock type (**Fig. 5a**): crater suevites show a moderate negative correlation (R^2 = 0.54, $p < 0.001$), with high CRS wt% tending to correspond with low $\delta^{34}S_{CRS}$, while impact melt breccias show no discernable relationship ($R^2 = 0.03$). TOC wt% varies from < 0.1% (*i.e.*, below detection limit [b.d.l.]) to 0.8%, but the majority of samples display low values; all but four of the 34 analyses have ≤ 0.3 wt% TOC. TOC wt% is consistently low in the samples with highest CRS

wt% (**Fig. 5b**)—specifically, all samples with CRS contents > 1.3 wt% (n = 15) also have TOC ≤ 0.1 wt%.

BSE imaging (**Fig. 6**) reveals that Fe-sulfides are mainly disseminated throughout the groundmass (*i.e.*, not in clasts) of both the crater suevite and the impact melt breccia. This observation is in agreement with previous petrographic and geochemical analyses of SUBO 18 (Reimold *et al.*, 2012; Reimold *et al.*, 2013), which revealed that these sulfides are predominantly pyrite of post-impact origin, with minor occurrences of sphalerite [(Zn, Fe)S] in melt particles. Morphologically, the vast majority of the observed pyrite is non-framboidal, regardless of sample depth. Only one ~100 μm^2 area of one sample (68.59 m) was observed to contain framboid-like morphologies, which are ~1 μm in diameter and fracture-filling.

4.2.2. Field Samples (Outer Suevite)

All three field samples of outer suevite display CRS contents of 10 mg/kg or less. As a result, isotope measurements were not performed on these samples. These values are notably below 0.04 wt%, the observed CRS minimum for crater suevite. TOC was ≤ 0.1 wt%, and TS was < 0.1 wt% for all outer suevite samples.

5. Discussion

5.1. Overview of sulfur geochemistry at the hydrothermal Ries crater lake

The SUBO 18 interval under investigation is composed of impact breccias that had hydrothermal fluids migrate through them en route to the water column of the Miocene Ries crater lake. The formation of secondary pyrite in the subsurface impact breccias likely had a direct influence on the S chemistry of the fluids that reached and accumulated in the overlying waters, and the chemistry of these lake waters is preserved in the sedimentary deposits of FBN 73. The strongest hydrothermal influence on lake water chemistry likely occurred during the basin's early evolution from transient playas to a permanent lake (*i.e.*, an interval of several 100 kyr that was likely coincident with the basal member extending into the early laminite member). The distinct geochemical differences between SUBO 18 and FBN 73 (**Fig. 2**) support this overarching interpretation. The lowest $\delta^{34}S_{CRS}$ values are sequestered in impact breccia, with the highest $\delta^{34}S_{CRS}$ values residing in the laminite member of the paleolake sediments. In a general sense, this relationship would be expected in order to satisfy isotopic mass balance. Past research suggests that meteoric waters (*i.e.*, supplied by a combination of groundwater and precipitation) and the materials that they weathered were likely the only significant sources of dissolved SO_4^{2-} to the lake for much of its history (Arp *et al.*, 2013a). During periods of hydrothermal activity, much of that SO_4^{2-} was apparently scavenged in the subsurface as sulfide, resulting in average CRS contents that are higher in the underlying impact breccias compared to sediments of the laminite member. Sulfate that was not scavenged in the subsurface would have become available to the lacustrine system via ascending hydrothermal fluids.

Within the crater lake ecosystem, as archived by FBN 73 and the carbonate mound samples, $\delta^{34}S$ was uniformly high. CAS data (**Fig. 4**) indicate that the SO_4^{2-} isotope composition of the water column ($\delta^{34}S_{CAS}$) during deposition of the laminite member ranged from 26.4‰ to 44.5‰, a spread similar to that of the $\delta^{34}S_{CRS}$ values of the FBN 73 laminite (17.5‰ to 45.1‰). Absolute concentrations of dissolved SO_4^{2-} in the lake water column cannot be directly inferred from measured CAS concentrations or $\delta^{34}S_{CAS}$ (Fichtner *et al.*, 2017; Gill *et al.*, 2008). However, given the depositional similarities of the carbonate mounds sampled in this study, we assert that comparisons of relative CAS concentrations, at least in a first-order sense, are valid. The strong anticorrelation between CAS concentrations and $\delta^{34}S_{CAS}$ values ($R^2 = 0.81$) suggests that high

extents of S sequestration in the subsurface impact breccias led to more positive $\delta^{34}S$ values of the water-column SO_4^{2-}. Furthermore, because the Wallerstein samples are older than those of the Goldberg mound, the $\delta^{34}S_{CAS}$ data of the carbonates fall on the same stratigraphically descending $\delta^{34}S$ trend defined by the laminite member. The slight differences between $\delta^{34}S_{CAS}$ and laminite $\delta^{34}S_{CRS}$ values therefore indicate small or insignificant fractionation events during the transformation of dissolved SO_4^{2-} (as captured by CAS) to mineral-phase sulfide (represented by CRS), or vice versa.

The data across the NR cores (**Fig. 3**) provide additional evidence that the general observed lake $\delta^{34}S$ trend represents a homogenous signal that existed throughout the basin and that $\delta^{34}S$ values are similar in magnitude across all phases measured (*i.e.*, CRS, CAS, bulk materials, and kerogen). The NR core data also extend the argument that, at least during deposition of the lower laminite member, sulfate with high $\delta^{34}S$ was distributed throughout the water column and in the sediments, with that S pool being preserved in the sediments with minimal net fractionation. This assertion is consistent with experimental studies that have demonstrated only small (< 4‰) $\delta^{34}S$ fractionation during the formation of both CAS from dissolved sulfate and pyrite from dissolved sulfide (Barkan *et al.*, 2020; Butler *et al.*, 2004), although some ^{34}S enrichment has been observed in sedimentary organic matter when compared to co-existing Fe-sulfides (*e.g.*, Kotuzov *et al.*, 2020).

In a model approach, Arp *et al.* (2013a) used the SO_4^{2-} concentrations found in local modern groundwaters (~0.85 mM; Winkler, 1972) and a dynamic impact breccia weathering scenario to show that water column SO_4^{2-} values were likely higher than 200 μM shortly after lake formation and remained that way for the remainder of the lake's lifetime (Arp *et al.*, 2013a; Füchtbauer *et al.*, 1977). Therefore, a concentration-dependent metabolic isotope effect, which can lead to small fractionations from MSR in a low SO_4^{2-} [below 200 μM] environment, appears unlikely (Crowe *et al.*, 2014; Habicht *et al.*, 2002; Harrison and Thode, 1958). However, near-quantitative MSR (*i.e.*, an extent that is indistinguishable in the rock record from a quantitative reaction)—leading to reservoir-effect-induced sulfide isotopic compositions that closely resemble those of the parent dissolved SO_4^{2-}—is plausible under the high organic productivity regime of the laminite member. Microbial sulfate reduction likely occurred in the lake sediments during early diagenesis and possibly in the water column during certain intervals (*i.e.*, euxinia), specifically in a saline hypolimnion with a sulfide surplus relative to Fe^{2+}, as indicated by the presence of thiophene biomarkers in the early laminite sediments (Arp *et al.*, 2013a; Barakat *et al.*, 1994; Barakat and Rullkötter, 1997; Rullkötter *et al.*, 1990).

The coincident, gradual decline in $\delta^{34}S_{CRS}$ throughout the remainder of FBN 73 could then be interpreted as reflecting a highly restricted, evaporitic lake with progressively decreasing contributions of hydrothermally derived SO_4^{2-} and progressively increasing contributions of SO_4^{2-} from karstic groundwater and surface weathering of Bunte Breccia (Arp *et al.*, 2013a). In any case, it is apparent that there was little-to-no observable S-isotope fractionation within the earliest subaerial lake itself. Thus, we interpret from the above data that the primary locus of fractionation (and therefore the source of both the maximum and minimum observed $\delta^{34}S$ values) was the subsurface hydrothermal system. The exact nature of the S isotope fractionation mechanism in the hydrothermal system, and its relevance as a biosignature, is more complex.

5.2. Mechanisms for the observed sulfur isotope variation

There are multiple lines of reasoning that can be used to assess the observed $\delta^{34}S$ variation at Ries Crater. MSR is often evoked as a means of explaining large differences in $\delta^{34}S$ values between

source sulfate and product sulfide [$\Delta^{34}S_{sulfate\text{-}sulfide}$], with offsets of up to 75‰ (Brunner *et al.*, 2005; Canfield *et al.*, 2010; Lyons and Gill, 2010; Sim *et al.*, 2011; Wortmann *et al.*, 2001). However, meteorite impacts can induce target rock temperatures well in excess of 130°C, exceeding the limits of life and possibly generating significant thermochemical sulfate reduction while using the reducing power of organic matter (Abramov and Kring, 2005; Ivanov, 2004; Machel, 2001; Osinski *et al.*, 2013). Thermochemical sulfate reduction has been shown to yield $\Delta^{34}S_{sulfate\text{-}sulfide}$ values of up to 21‰; this can confound interpretations that assign S-isotope fractionations to MSR, specifically in cases where $\delta^{34}S$ variations are smaller than 21‰ in rocks exposed to temperatures above 100°C (Machel *et al.*, 1995; Machel, 2001; Ohmoto and Goldhaber, 1997; Watanabe *et al.*, 2009). Additionally, theoretical work indicates that hydrothermal activity can lead to large equilibrium fractionations between aqueous SO_4^{2-} and H_2S—*e.g.*, $\Delta^{34}S_{SO_4^{2-}\text{-}H_2S}$ = 43.4‰ at 100°C (Eldridge *et al.*, 2016; Marini *et al.*, 2011; Ohmoto and Goldhaber, 1997; Sakai, 1968). Equilibrium S fractionation is typically considered for magmatic hydrothermal systems, but impact events also provide a plausible setting for this effect, depending on crater size, target rock composition, and fluid chemistry (Abramov and Kring, 2007; Franz *et al.*, 2017; Ivanov, 2004; Kirsimäe and Osinski, 2012; Marini *et al.*, 2011; Osinski *et al.*, 2013). Each of these scenarios (*i.e.*, MSR, TSR, and equilibrium fractionation) warrants individual evaluation, as well as consideration for the potential simultaneous or sequential occurrence of two or more fractionation mechanisms.

5.3. Microbial sulfate reduction

If the $\delta^{34}S$ data are viewed in the absence of the full system context, MSR is the most straightforward way to reconcile the $\delta^{34}S_{CRS}$ difference between the highest paleolake sedimentary samples and average impact breccia values (Δ = 61‰; **Fig. 2, Supplemental Table 1**). Hydrothermal activity does not preclude MSR: optimal growth rates for hyperthermophilic MSR Bacteria can be at temperatures as high as 83°C, with an observed upper limit of 90°C (*Thermodesulfobacterium geofontis*; Hamilton-Brehm *et al.*, 2013), while MSR Archaea also show optimal growth at temperatures as high as 83°C (*Archaeoglobus fulgidus*; Stetter 1988; Stetter *et al.* 1987) but can apparently function at temperatures ~100°C (Elsgaard *et al.*, 1994; Jørgensen *et al.*, 1992; Weber and Jørgensen, 2002). Canfield *et al.* (2000) measured MSR $\delta^{34}S$ fractionation from Guaymas Basin sediments sampled at 85°C and found $\Delta^{34}S_{sulfate\text{-}sulfide}$ of 13‰ to 28‰, comparable to results from pure thermophilic cultures (Böttcher *et al.*, 1999). This fractionation is notably smaller than that observed in some isolates from mesophilic environments (*i.e.*, > 60‰ in those measured by Canfield *et al.*, 2010, and Sim *et al.*, 2011). Taken together, these studies point to TSR or hydrothermal equilibrium as being the dominant S-fractionation mechanisms in geologic settings with temperatures > 100°C (Machel, 2001) and imply that, from a $\delta^{34}S$ perspective, it becomes increasingly difficult to distinguish between MSR and TSR as this temperature range is approached.

Appraisals of hyperthermophilic MSR viability aside, the lack of observed framboidal pyrite (associated with organics or otherwise) in favor of fracture- and/or void-filling forms makes possible biological origins ambiguous. In the single observed area where framboid-like pyrite is found (**Fig. 6b**), it is present in fracture fills. Indeed, these forms observed in SUBO 18 may not be true framboids in the sense that they do not show organized or disorganized clustering. They can instead be described as linked, near-equidimensional microcrystals. Even if we assume that all observed framboid-like pyrite was of bacterial origin, despite the variety of abiotic framboid formation mechanisms (Ohfuji and Rickard, 2005), these pyrites would be insignificant in terms of their overall contribution to $\delta^{34}S$ mass balance because they compose only a small portion of

the total pyrite. The potential for morphological overprinting of pyrite framboids due to hydrothermal activity (Nozaki *et al.*, 2020) furthers ambiguity and highlights a broader issue for sulfide biogenicity, as hydrothermalism is generally considered a relevant feature for origin of life hypotheses on Earth as well as the search for life elsewhere (Deamer *et al.*, 2019; Hendrix *et al.*, 2019; Schwenzer and Kring, 2009). Hydrothermal activity is known to have been a feature of many impact craters on Earth and Mars (Osinski *et al.*, 2013).

Contextual geochemical trends also contribute to MSR uncertainty. TOC wt% in the SUBO 18 samples is uniformly low, and a TOC wt% vs CRS wt% crossplot (**Fig. 5b**) shows low TOC wt% corresponding to high CRS wt%. This trend is the reverse of that typical of MSR, where higher TOC contents facilitate greater pyrite precipitation (*e.g.*, Westrich and Berner, 1984). This reasoning also applies when scrutinizing the trend seen in suevite samples specifically (**Fig. 5a**), where higher CRS wt% corresponds to lower $\delta^{34}S_{CRS}$; greater rates of MSR and thus pyrite formation should impart smaller fractionations (Canfield, 2001; Kaplan and Rittenberg, 1964)—but the opposite is observed. Rather than invoking biology, these data may be better interpreted within the framework of post-impact TSR at temperatures exceeding 100°C.

5.4. Thermochemical sulfate reduction

Thermochemical sulfate reduction, like MSR, can consume organic carbon, facilitating pyrite formation and establishment of the lake's well-documented high alkalinity (Arp *et al.*, 2013a; Füchtbauer *et al.*, 1977; Stüeken, Tino *et al.*, 2020). Importantly, TSR has been shown to be capable of fully consuming reactive carbon compounds in experimental settings (Meshoulam *et al.*, 2016), allowing for the observed high CRS wt% with low TOC wt% relationship in SUBO 18 (**Fig. 5b**). The net mass balance schematic thought to drive TSR is as follows (Machel, 1987; Machel, 2001):

$$SO_4^{2-} + \text{hydrocarbons} \rightarrow H_2S(HS^-) + HCO_3^-(CO_2) + H_2O + \text{altered hydrocarbons} + \text{solid bitumen}, \quad (1)$$

where speciation within the CO_2-H_2O and H_2S-H_2O systems is pH- and temperature-dependent (*e.g.*, Ohmoto and Goldhaber, 1997). There are multiple pathways that can play a role within this overall scheme, including an autocatalytic process involving H_2S consumption and generation (Orr, 1974; Zhang *et al.*, 2008) and the potential necessity for Mg or Ca (Ma *et al.*, 2008) in facilitating initial H_2S generation at the pH range (~6.5-8.5) of most TSR environments (Collins, 1975; Machel *et al.*, 2001). This pH range is compatible with values suggested for the Ries hydrothermal fluids (Muttik *et al.*, 2011; Osinski, 2005). Although fractionations associated with TSR do not appear to exceed the ~21‰ offset suggested in the $\delta^{34}S$ data compiled by Ohmoto and Goldhaber (1997) or generated experimentally by Watanabe *et al.* (2009), this value is not substantially smaller than what has so far been observed in (hyper)thermophilic MSR cultures (*e.g.*, Böttcher *et al.*, 1999; Canfield *et al.*, 2000; Davidson *et al.*, 2009; Habicht *et al.*, 2005; Mitchell *et al.*, 2009).

Rayleigh fractionation in a closed-system with respect to reactant SO_4^{2-} (and open for product H_2S to be removed as pyrite or volatilized out of the system; *e.g.*, Hartmann and Nielsen, 2012) illustrates how distillation effects may have enhanced isotopic discrepancies within the crater lake system (**Fig. 7; Fig. 8**), where:

$$\delta_{reactant(t)} = (\delta_{reactant(t=0)} + 1000) \cdot f^{(\alpha_{product\text{-}reactant} - 1)} - 1000 \quad (2)$$

$$\alpha = (1000 + \delta^{34}S_{product})/(1000 + \delta^{34}S_{reactant}) \quad (3)$$

and the δ value of total product molecules is approximated by:

$$\delta_{\Sigma product} = (\delta_{reactant(t=0)} - f \cdot \delta_{reactant(t)})/(1- f) \quad (4)$$

Within this framework, the observed maximum $\delta^{34}S_{CRS}$ in the lake sediments ($\geq$ 45.1‰) and the mean $\delta^{34}S_{CRS}$ of SUBO 18 breccia (-15.8‰; represented here by the cumulative sulfide $\delta^{34}S$—or $\delta^{34}S_{\Sigma H_2S}$—value) can be satisfied via distillation. For example, when applying an initial $\delta^{34}S_{SO_4^{2-}}$ of 0‰, 74.1% of the original SO_4^{2-} pool must be removed with an enrichment factor [ε, where $\varepsilon = \delta^{34}S_{product} - \delta^{34}S_{reactant} \approx 1000\ln\alpha_{product\text{-}reactant}$] of ε = -32.8‰ ($\alpha \approx 0.9672$) in order to satisfy empirical observations (**Fig. 7a**). This enrichment factor is in excess of that for TSR (ε = -21‰) and higher than observations for cultured hyperthermophilic MSR (ε = -28‰). Alternatively, assuming a maximum TSR fractionation of ε = -21‰ ($\alpha \approx 0.9790$) in the same scenario generates $\delta^{34}S_{SO_4^{2-}}$ = 45.1‰ and $\delta^{34}S_{\Sigma H_2S}$ = -6.2‰ after reducing 87.8% of the original SO_4^{2-} pool (**Fig. 7b**). We use the maximum empirical ε value as a test case because the search for life elsewhere warrants a conservative approach to minimize the risk of a false positive. Similar ε values have been observed experimentally at 150°C (ε = -20.8‰; Watanabe *et al.*, 2009), which is within the temperature range of the main alteration stage of Ries' impact breccias (100-200°C; Osinski, 2005). Shifting the initial $\delta^{34}S_{SO_4^{2-}}$ value in the negative direction allows for TSR results that track the entire dataset more closely. Thus, an initial $\delta^{34}S_{SO_4^{2-}}$ of -11.4‰ results in a $\delta^{34}S_{\Sigma H_2S}$ value of -15.7‰ with a $\delta^{34}S_{SO_4^{2-}}$ of 45.1‰ at 92.9% SO_4^{2-} removal. This scenario would require the mixing of isotopically light SO_4^{2-} into the hydrothermal SO_4^{2-} reservoir. A plausible source of isotopically light sulfate is the oxidative weathering of pyrite within country rocks and/or impactites, including the Toarcian Posidonia shale, which is known to have contributed organic matter to Ries impact breccias (Hofmann *et al.*, 2001). Previously measured $\delta^{34}S_{pyrite}$ from the Posidonia shale range from -7.7 to -44.5‰ (Berner *et al.*, 2013). Various other target rock and regional S-bearing phases, including Jurassic carbonates (Reinhold, unpublished data) and Triassic arkoses (Nielsen, 1985; von Gehlen and Nielsen, 1985), display similarly low $\delta^{34}S$ values. Impact redistribution and oxidation of such materials, particularly via groundwater flow, may have lowered the $\delta^{34}S_{SO_4^{2-}}$ being fed into the hydrothermal system to $\delta^{34}S_{SO_4^{2-}} \leq$ -11.4‰ (*i.e.*, consistent with the Rayleigh model presented above). While the pyrite in Posidonia shale, for example, is biogenic, naturally occurring abiotic pyrite with $\delta^{34}S \leq$ -11.4‰ (*e.g.*, Goldfarb *et al.*, 1991; Ohmoto and Goldhaber, 1997) could comprise the target rock of an impact crater on ancient Earth or Mars. Our model (**Fig. 8**) therefore explores a valid analog scenario.

The Rayleigh distillation scenarios above assume an ideal closed system and therefore can only provide a limited reconstruction of what was a highly dynamic environment (**Fig. 8**). Much of the earliest hydrothermal fluid was likely derived from groundwaters migrating into the hydrostatic void generated by the impact event (Osinski, 2005). Surface water would have percolated back downward into the breccia (Osinski, 2005) and tenuously balanced the upward movement of groundwater, particularly after reaching a hydrostatic equilibrium (there is no evidence of outlet formation at Ries crater). Thus, while Ries is not a theoretically ideal closed system, SO_4^{2-} anions would have had prolonged exposure to subsurface hydrothermal circulation. In any case, extensive Rayleigh distillation appears to have occurred: even the highest observed hyperthermophilic MSR fractionation (ε = -28) would require significant closed-system SO_4^{2-} removal (> 75%) to mimic the observed data.

It should be noted that an all-encompassing numerical solution that assumes the Ries crater to be a completely closed system with regards to $\delta^{34}S$ is not necessary to explain our observations. This is because temporal constraints on the intensity of hydrothermal activity during the paleolake interval that hosts $\delta^{34}S$ values of > 40‰ are limited. It is possible, for instance, that the $\delta^{34}S_{SO_4^{2-}}$

composition of the lake at that time reflects the latest possible stages of hydrothermal activity, when only the uppermost suevite was interacting with the lake surface water. The change in $\delta^{34}S_{\Sigma H_2S}$ through time may be reflected in the suevite $\delta^{34}S_{CRS}$ trend, which increases moving up core. This argument allows for a scenario discussed above, where TSR generates $\delta^{34}S_{SO_4^{2-}}$ of 45.1‰ and $\delta^{34}S_{\Sigma H_2S}$ of -6.2‰ from initial $\delta^{34}S_{SO_4^{2-}}$ of 0‰ and could explain the relatively elevated $\delta^{34}S_{CRS}$ of the two uppermost suevite samples (which show values of -7.1‰ and -10.0‰). For this to occur, S would need to permanently escape the restricted basin, which can happen via H_2S volatilization. If the early laminite member waters were euxinic (Arp *et al.*, 2013a; Barakat *et al.*, 1994; Barakat and Rullkötter, 1997; Rullkötter *et al.*, 1990), H_2S derived from the hydrothermal system could have been transported to the lake's water column. Water-column sulfide is susceptible to volatilization (Fry *et al.*, 1986; Reese *et al.*, 2008). An example is the modern Salton Sea in California, USA, where H_2S escapes to the atmosphere during seasonal mixing in a process that has been projected to remove ~24% of the basin's dissolved H_2S annually (Reese *et al.*, 2008). While this effect imparts only minor fractionation ($\varepsilon_{gas\text{-}aqueous}$ = -1.6‰ to 3.0‰; see Baune and Böttcher, 2010; Fry *et al.*, 1986; Sim *et al.*, 2019), it nonetheless allows for the isotopic evolution of a restricted basin's sulfur reservoir on geologic timescales. This is because a proportion of the S derived from hydrothermal activity and isotopic distillation could have escaped via volatilization relatively early in the lake's history. If this was followed by increased relative input and mixing of non-hydrothermal, meteoric S (with its lower $\delta^{34}S$ composition), then the elevated early lacustrine $\delta^{34}S$ signal would be effectively diluted over time. The implication is that during formation of the lightest pyrite, $\delta^{34}S_{SO_4^{2-}}$ of < 45.1‰ may have been generated but is only briefly recorded in the rock record (*i.e.*, during the transition from the basal member into the laminite member, where paleolake $\delta^{34}S_{CRS}$ values shift from -5.2‰ to 41.9‰ over the core depths of 260.5m–248.5m). As the basin evolved, the restricted recycling of high $\delta^{34}S_{SO_4^{2-}}$ could have resulted in the simultaneous occurrence of the highest suevite $\delta^{34}S_{CRS}$ and the highest paleolake $\delta^{34}S$ values (Δ = 52.8‰, where $\delta^{34}S_{SO_4^{2-}}$ = 45.1‰ and $\delta^{34}S_{\Sigma H_2S}$ = -7.7‰). This spread can occur from TSR removing ~89% of a limited pool of SO_4^{2-} with an initial $\delta^{34}S_{SO_4^{2-}}$ value of -1.7—a plausible value for groundwater SO_4^{2-}, even without the likely mixing of an isotopically lighter SO_4^{2-} source such as oxidized pyrite of the Posidonia shale and/or other pyrite-bearing Jurassic and Triassic formations of the target rocks (Arp *et al.*, 2021b). In light of the above discussion, we assert that TSR was as likely as MSR to have been the primary $\delta^{34}S$ fractionation mechanism in Ries crater.

5.5. Hydrothermal equilibrium isotope fractionation

The near-absence of organics associated with the most sulfide-enriched impact breccia samples may imply a role for hydrothermal equilibrium fractionation. After the exhaustion of reactive organic matter via TSR, equilibrium fractionation between aqueous S-bearing phases has been shown to occur (Meshoulam *et al.*, 2016). The timescales needed for such an equilibration are highly dependent on temperature, pH, and the total concentration of S species [ΣS] (Ohmoto and Goldhaber, 1997; Sakai, 1968). According to the equations presented in Ohmoto and Goldhaber (1997), a hydrothermal solution (T = 100°C, pH = 7, ΣS = 0.01 molal) would take ~407 kyr to reach 90% of isotope exchange equilibrium (*i.e.*, indistinguishable from an equilibrium state). At that temperature, the equilibrium fractionation for between SO_4^{2-} and H_2S has a $1000ln\alpha$ value of about 43‰, with SO_4^{2-} being substantially enriched in ^{34}S (Eldridge *et al.*, 2016; Sakai, 1968). The subsequent equilibration of H_2S and HS^-, which is an expected occurrence at circumneutral-to-basic pH, results in a $1000ln\alpha$ value of 2.5, where H_2S has a higher $\delta^{34}S$ than HS^- (Eldridge *et al.*, 2016; Sakai, 1968). While the hydrothermal fluid composition described above is

broadly consistent with the results from previous studies of the Ries crater system (*e.g.*, Arp *et al.*, 2013b; Muttik *et al.*, 2010; Osinksi, 2005; Sapers *et al.*, 2017), generating such a large fractionation would require fluid temperatures at ~100°C for the entirety of the protracted equilibration time. Further, changes to single parameters of the fluid composition profoundly decrease the likelihood of this fractionation. Shifting the pH to ~9, which is compatible with the pH range suggested for the Ries system based on boron isotope measurements (Muttik *et al.,* 2011), would increase the time necessary for an equilibration from ~407 kyr to an impossible ~869 Gyr. Decreases in ΣS by a factor of 10 also increase the time to equilibrium by a factor of 10 (Ohmoto and Goldhaber *et al.*, 1997). Due to these rigid theoretical constraints, if hydrothermal equilibrium were ever reached at Ries crater, it would have been brief and occurred at temperatures where the equilibrium fractionation is much smaller (*e.g.*, at 300°C, $1000ln\alpha = 19.8$; Eldridge *et al.*, 2016). Such effects would be transient and likely overprinted beyond interpretation by larger, non-equilibrium fractionations caused by TSR or MSR. However, this remains a viable abiotic mechanism in acidic and/or high ΣS fluid environments where reductant scarcity prohibits non-equilibrium fractionation mechanisms.

6. Conclusion and Astrobiological Implications

In the present study, we tested the viability of stable sulfur isotopes as a biosignature in impact crater lakes through a detailed investigation of the Miocene Ries crater, which serves as an analog to early habitable locations on Mars and Earth. At Ries, elevated temperatures sustained by impact-induced hydrothermal activity allowed for the possibility of S isotope fractionation mechanisms that are rare in mesophilic environments (where $\delta^{34}S$ variation > 21‰ is often representative of microbial S cycling). After examining the observed $\delta^{34}S$ spread of ~77‰ at the Ries crater, we contend that TSR was at least as likely as MSR to have been the primary $\delta^{34}S$ fractionation mechanism (**Fig. 8**). This conclusion is further supported by multiple lines of evidence, including impact breccia with TOC wt% versus CRS wt% and $\delta^{34}S_{CRS}$ versus CRS wt% relationships that are atypical of biological controls, as well as ambiguous pyrite textures. The hydrothermal system apparently dominated S isotope fractionation, as there is evidence (in the form of near-equivalent $\delta^{34}S$ in CRS, CAS, bulk-S, and kerogen-S samples) that lacustrine S cycling imparted little-to-no $\delta^{34}S$ fractionation during deposition of the most ^{34}S-enriched lacustrine pyrite (45‰). We have shown that a potential source of isotopically light SO_4^{2-} (*e.g.*, oxidized pyrite of the Posidonia shale, or from other Jurassic and/or Triassic formations) from the catchment area of the lake would have allowed, via Rayleigh distillation of residual SO_4^{2-}, for TSR fractionation events of 21‰ to result in $\Delta^{34}S_{SO_4^{2-}\text{-}H_2S}$ distributions that match the observed Ries $\delta^{34}S$ spread. Additionally, spatiotemporal uncertainties inherent to impact-induced hydrothermal activity imply that $\delta^{34}S$ turnover via mechanisms such as H_2S volatilization is possible at the Ries crater given extensive timescales, regardless of its closed-basin nature.

Our overarching assessment that wide-ranging $\delta^{34}S$ in impact crater lakes need not be biological is in general agreement with *in-situ* Curiosity rover findings (Franz *et al.*, 2017), although the specified mechanisms differ. Hydrothermal equilibration of aqueous S species at temperatures ~100°C is unlikely at Ries given constraints involving elevated fluid pH and hydrothermal activity duration (several 100 ky) (Arp *et al.*, 2013b; Ohmoto and Goldhaber, 1997). However, this remains a viable fractionation mechanism at Gale crater, where fluid pH appears to have been acidic-to-circumneutral, and the crater's larger diameter (154 km) implies longer-lasting hydrothermal activity (Abramov and Kring, 2005; Berger *et al.*, 2017; McLennan *et al.*, 2013; Rampe *et al.*, 2020). Our study, however, suggests that impact-induced TSR of abiotically derived

organic matter should also be a considered S-fractionation mechanism at Gale, Jezero, and other ancient craters on Mars and Earth. Exogenous delivery of abiotic organics may have been relatively widespread early in our solar system's lifetime (Sandford *et al.*, 2020), and it is plausible that there was/is a subsurface abiotic organic reservoir on Mars (Eigenbrode *et al.*, 2018; Yang *et al.*, 2020) available to be incorporated into breccia during impact events and subsequently used as a reductant for TSR. TSR could have also proceeded on ancient Mars via alternative reducing species such as dissolved H_2 (Cai *et al.*, 2022; Wordsworth *et al.*, 2021) and has previously been proposed to explain the multiple sulfur isotope distribution of pyrite in Martian meteorite NWA 7533 (Lorand *et al.*, 2020). Therefore, even with our multitude of well-preserved samples, wet chemical techniques, and Earth-bound instrumentation, our wide-ranging (> 21‰) $\delta^{34}S$ data from an impact crater paleolake suggest that biological processes need not be involved. In other words, wide $\delta^{34}S$ ranges can be abiological, and overarching geologic context is essential to any interpretation of such data. Thus, the potential ambiguities of sulfur isotope composition as a biosignature should be recognized in future studies of crater systems on Mars and Earth. Ultimately, any convincing arguments for past life on Mars or elsewhere within or beyond our solar system would likely have to be built on multiple parameters viewed within a comprehensive context.

Acknowledgement

Special thanks to the laboratory of Professor Maryjo Brounce (UCR) for their generous sharing of lab space and instrument time for SEM analyses. For the purpose of open access, the authors have applied a CC-BY copyright license to any Author Accepted Manuscript version arising.

Data and Materials Availability

All data reported in this article are included in Supplementary Tables S1–S3. All data needed to evaluate the conclusions in the article are present in the article and Supplementary Materials. Additional data or information related to this article may be requested from the authors.

Authors' Contributions

C.J.T., E.E.S., and T.W.L. developed the project. C.J.T., E.E.S., T.W.L., and G.A. collected the samples. C.J.T. and M.E.B. carried out the sample preparation and analyses with support from S.M.B. C.J.T. wrote the article with contributions from all authors.

Author Disclosure Statement

The authors declare that the research was conducted in the absence of any commercial or financial relationships that could be construed as a potential conflict of interest.

Funding Information

NASA Fellowship in support of C.J.T. under Cooperative Agreement No. 80NSSC19K1739 issued through the NASA Office of STEM Engagement. Funding was provided to T.W.L. through the NASA Astrobiology Institute under Cooperative Agreement No.

NNA15BB03A issued through the Science Mission Directorate and the NASA Interdisciplinary Consortia for Astrobiology Research (ICAR). E.E.S. acknowledges funding from a NERC Frontiers grant (NE/V010824/1). Samples from drillcores NR-10, NR-20, NR-30, and NR-40 provided with permissions by BEB (now ExxonMobile). M.E.B. wishes to thank Professor Jürgen Rullkötter (ICBM Oldenburg) for access to the NR samples. Samples from Nö 1973 (FBN 73) and Enkingen (SUBO 18) provided by the Geological Survey of the Bavarian Environmental Agency (Dietmar Jung).

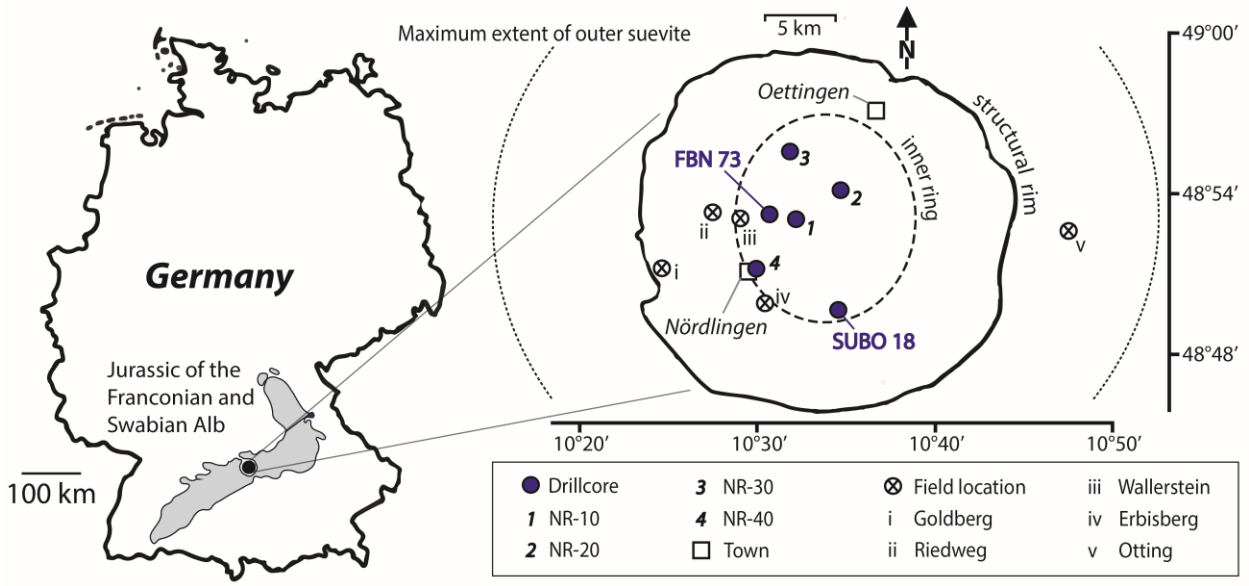

Figure 1 Geographical context for Ries crater, including the locations of all drill core and field sites sampled or referenced in this study. Adapted from Arp *et al.* (2013a) and Stöffler *et al.* (2013).

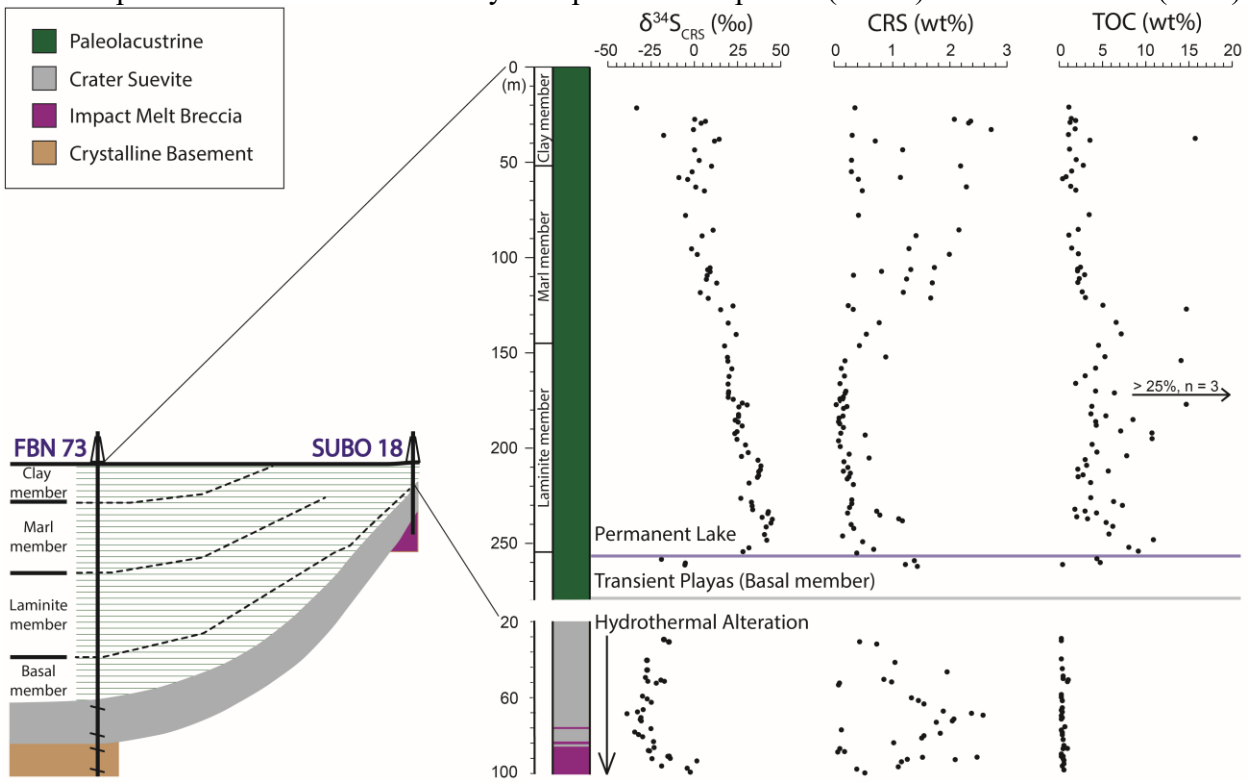

Figure 2 Stratigraphic trends of the FBN 73 and SUBO 18 drill cores, connected to a simplified diagram of their relative positions within Ries crater's concave structure. The depths used for bounding the four sedimentary units (members) of FBN 73 are from Füchtbauer *et al.* (1977), and the dashed stratigraphic correlation markers are adapted from Arp *et al.* (2021). Lithostratigraphy of SUBO 18 is adapted from Reimold *et al.* (2012). Angular lines near the base of the visual representation for FBN 73 represent breaks in stratigraphy and thus a deviation from relative scale at depths below 314.3 meters.

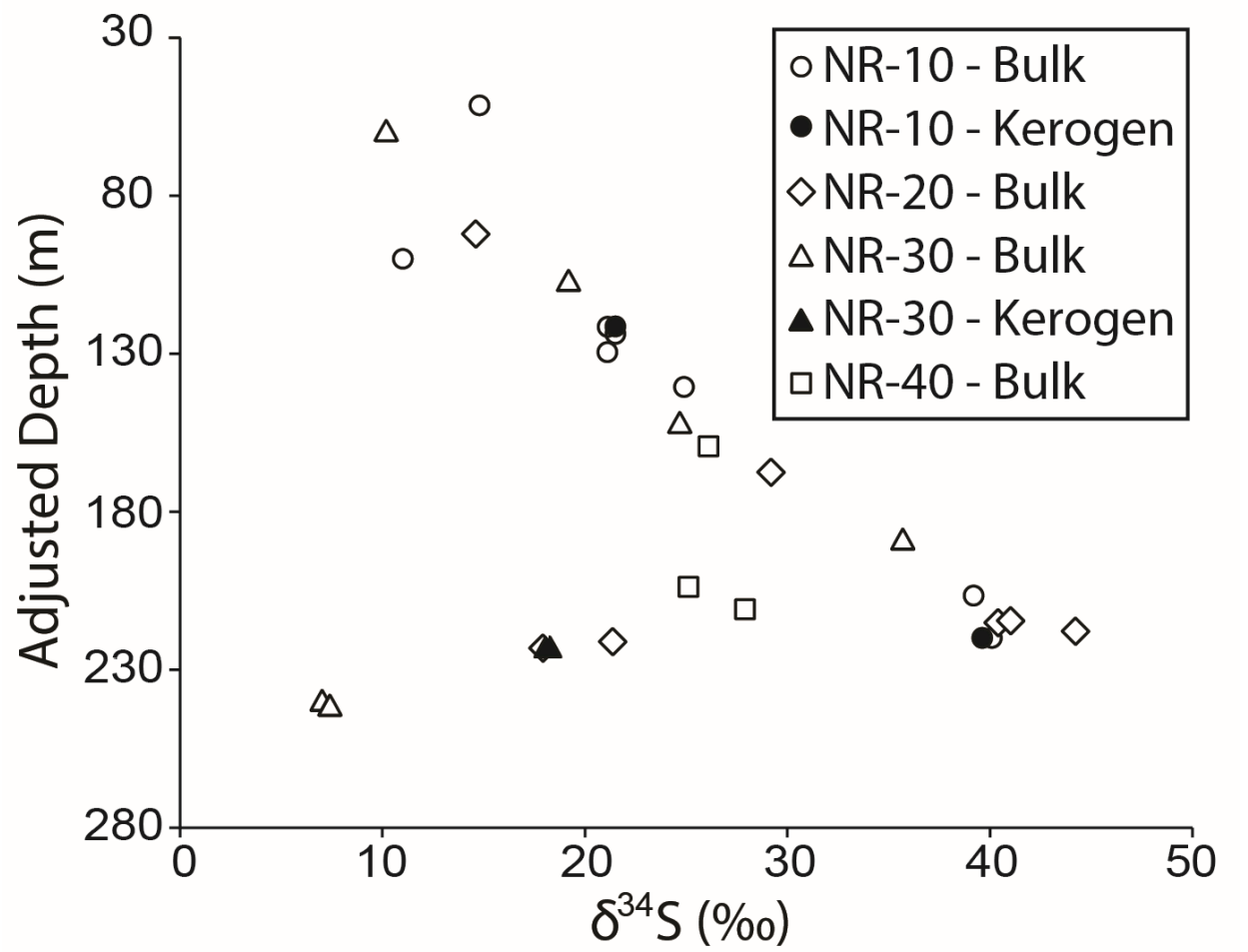

Figure 3 $\delta^{34}S$ data from bulk and kerogen analyses across the sedimentary paleolake intervals of four drill cores (NR-10, NR-20, NR-30, and NR-40) from within the inner ring of Ries crater. Sample depths were adjusted based on vertical trends, using the unadjusted NR-30 sample depths as a fixed reference point.

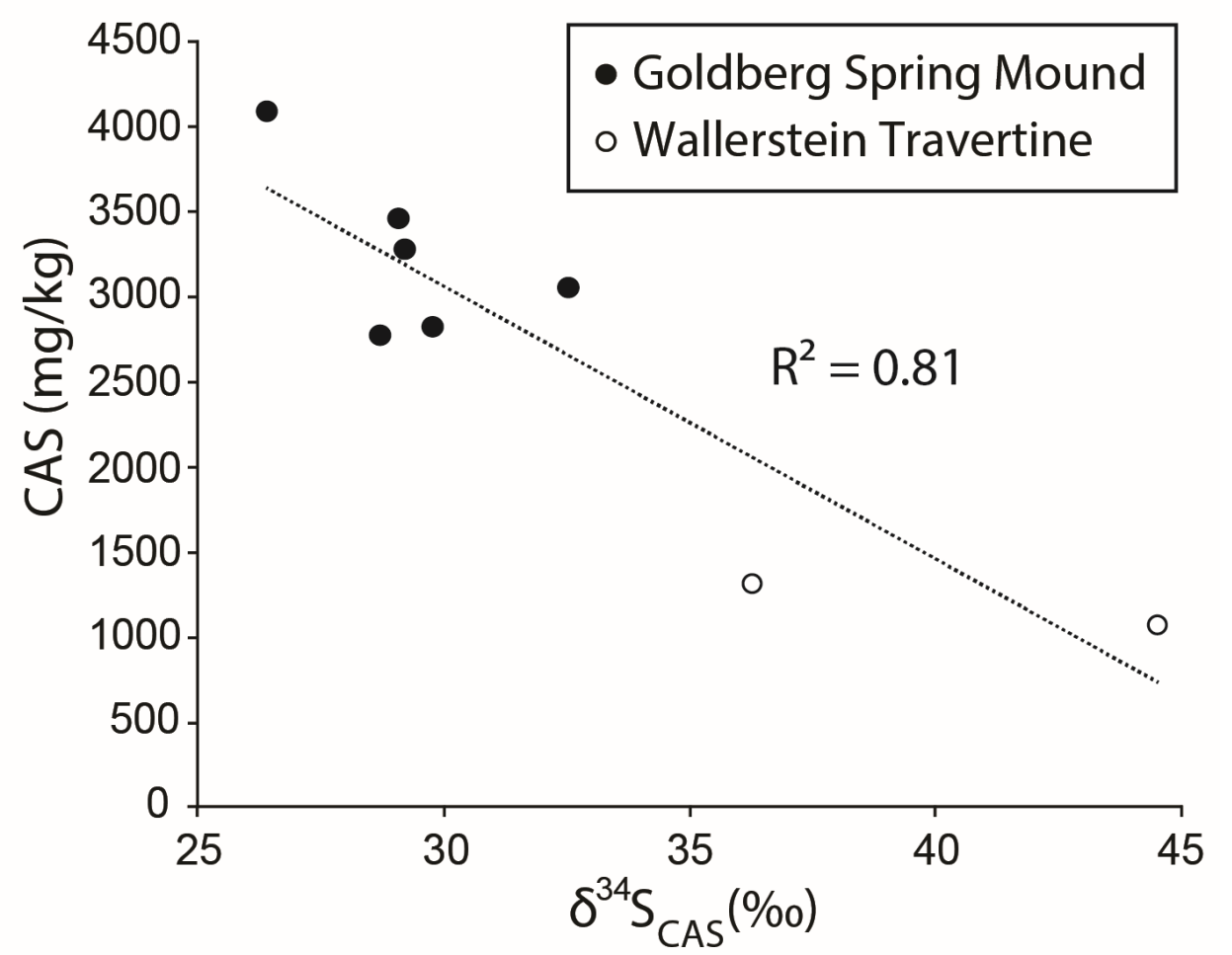

Figure 4 CAS (mg/kg) vs. $\delta^{34}S_{CAS}$ (‰) scatterplot composed of data generated from the Goldberg and Wallerstein carbonate mounds. The negative relationship with a strong coefficient of determination indicates that the highest $\delta^{34}S_{CAS}$ values were generated during intervals where the lake water had relatively low SO_4^{2-} concentrations.

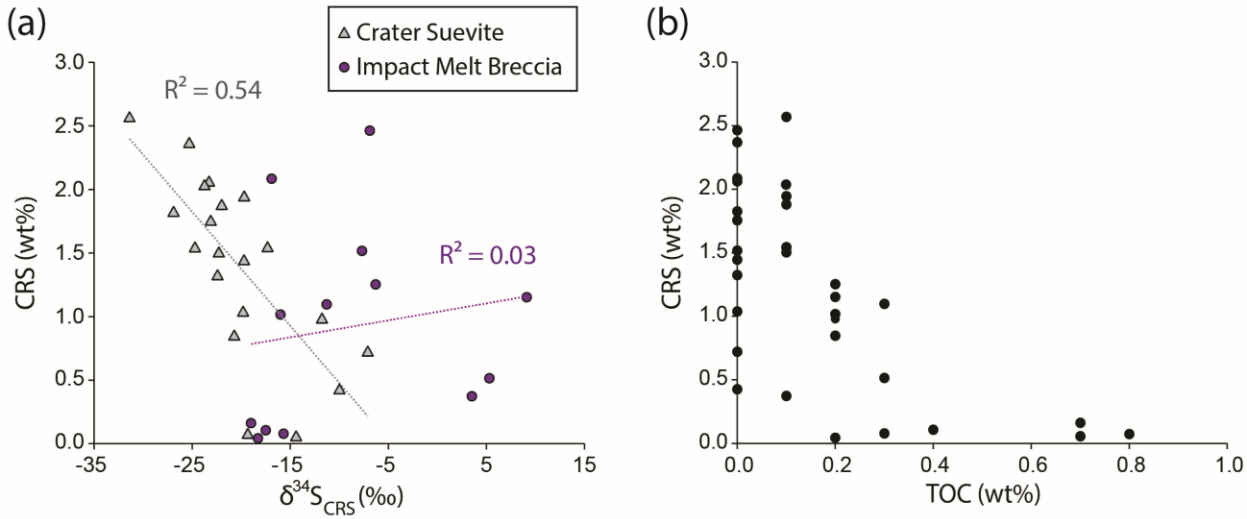

Figure 5 Scatterplots of SUBO 18 data. (a) There is a moderate relationship for CRS wt% versus $\delta^{34}S_{CRS}$ in crater suevite samples, but no relationship between these variables in impact melt breccia samples. (b) An apparent low TOC threshold is observed for the highest CRS contents, where all breccia samples with > 1.3 wt% CRS also have TOC ≤ 0.1 wt%.

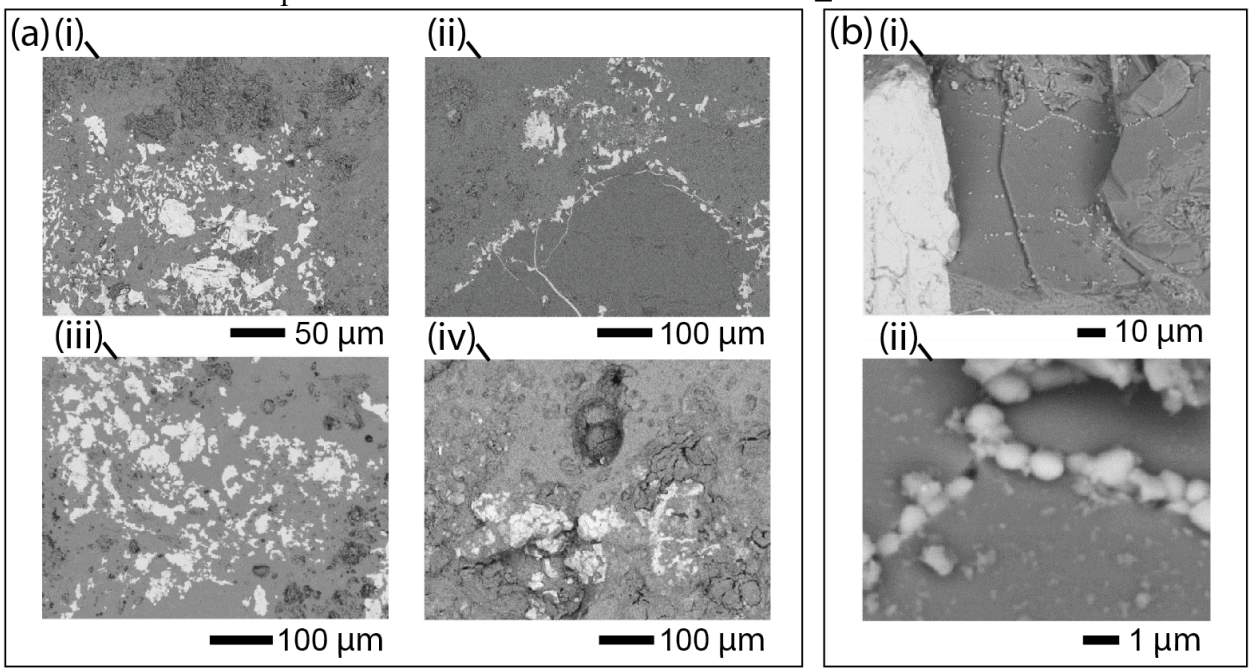

Figure 6 BSE Imaging data of polished SUBO 18 billets. (a) Images from four different depths show pyrite morphologies that are non-framboidal in nature. Depths: (i) 96.11 m, (ii) 90.93 m, (iii) 68.59 m, (iv) 30.75 m. (b) The only observation of framboid-like morphologies among the samples (shown at two different magnifications), where they (i) are filling fractures and (ii) are approximately 1 µm in diameter. They could alternatively be described as linked, near-equidimensional microcrystals. Both (i) and (ii) are at sample depth 68.59 m.

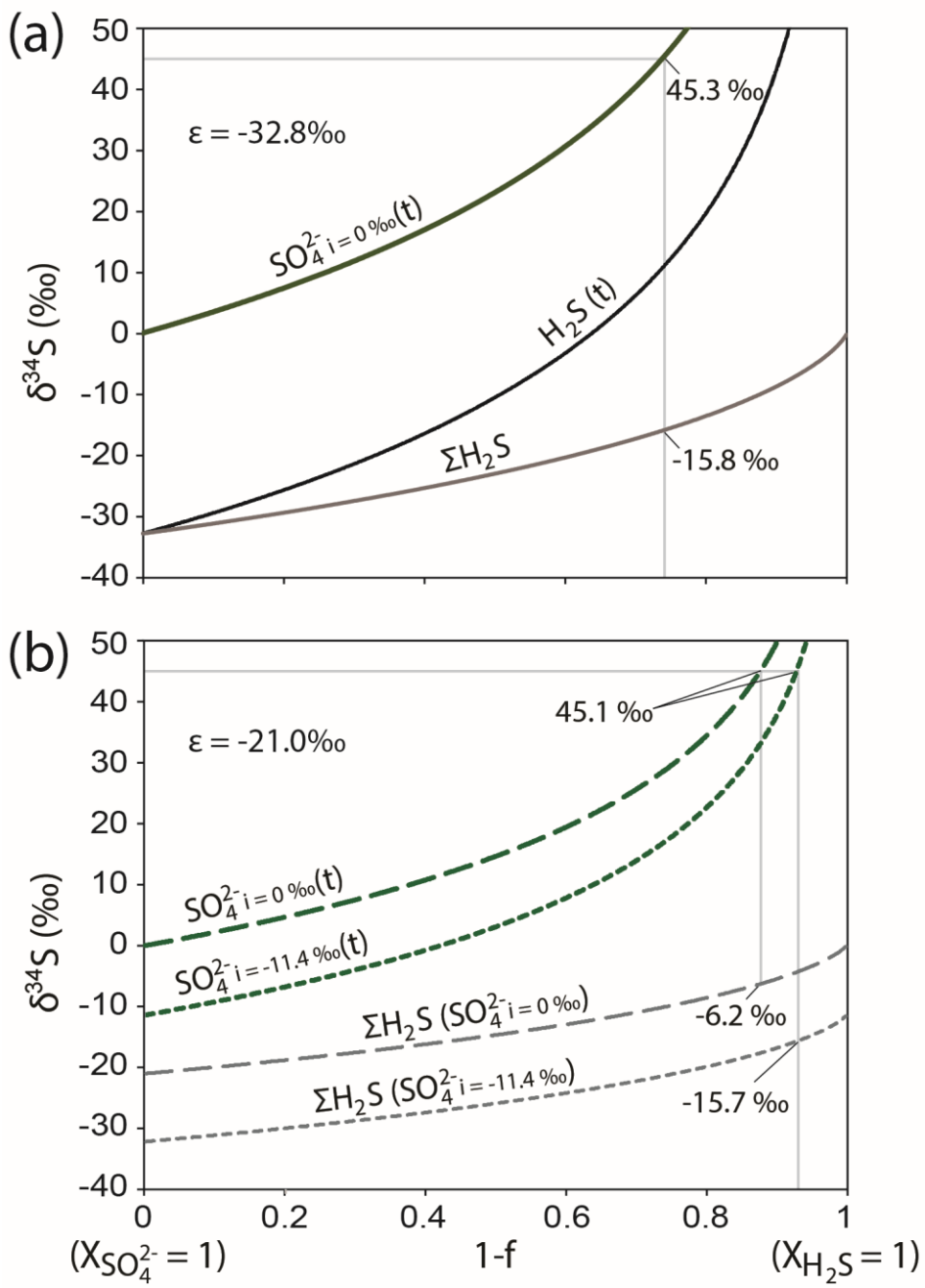

Figure 7 Rayleigh fractionation of stable S isotope ratios under multiple example starting conditions. (a) Using an initial $\delta^{34}S_{SO_4^{2-}}$ of 0‰ with an MSR-like enrichment factor of ε = -32.8‰ satisfies the maximum $\delta^{34}S_{CRS}$ observed in the lake sediments (≥ 45.1‰) with a $\delta^{34}S_{\Sigma H_2S}$ equal to the average SUBO 18 breccia $\delta^{34}S_{CRS}$ (-15.8‰). (b) Under a maximum TSR scenario (ε = -21.0‰) the initial SO_4^{2-} composition dictates whether the full observed isotopic range is expressed. An initial $\delta^{34}S_{SO_4^{2-}}$ of 0‰ results in $\delta^{34}S_{\Sigma H_2S}$ values ($\delta^{34}S_{\Sigma H_2S}$ = -6.2‰) that are higher than the average breccia $\delta^{34}S_{CRS}$ but within 1‰ of the suevite maximum ($\delta^{34}S_{CRS}$ = -7.1‰). Shifting the initial $\delta^{34}S_{SO_4^{2-}}$ value to -11.4‰, reflecting the input of light SO_4^{2-} (such as that sourced from oxidative pyrite weathering), satisfies the maximum $\delta^{34}S_{CRS}$ observed in the lake sediments with a co-occurring $\delta^{34}S_{\Sigma H_2S}$ that approximates the average SUBO 18 breccia $\delta^{34}S$.

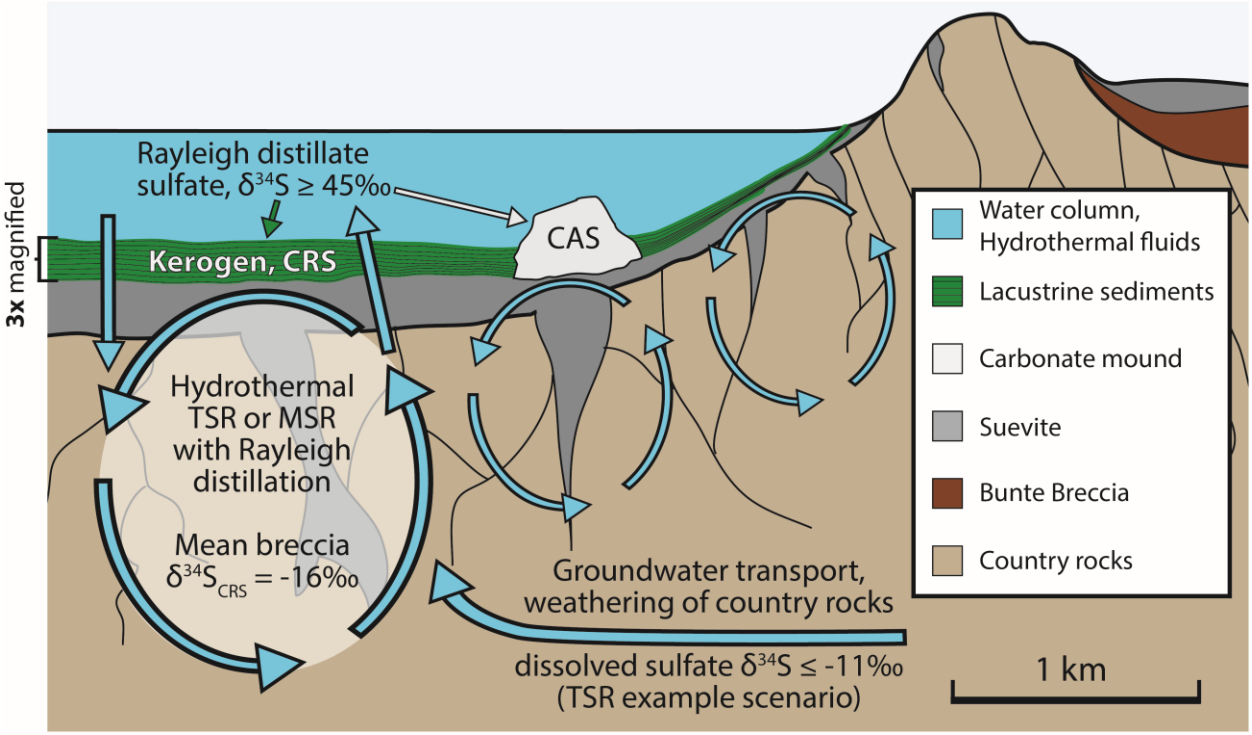

Figure 8 A proposed schematic of sulfur isotope fractionation at Ries crater during the earliest permanent lacustrine phase (late basal member into early laminite member). The primary locus of fractionation is within the subsurface hydrothermal system (fluid circulation indicated by blue arrows). The S system is initially fed by SO_4^{2-} primarily derived from the oxidative weathering of sulfide in country rocks that include impactites. Subaerial lake waters also percolate downward into the circulating fluids. In a TSR scenario (as described in **Section 5.4** and visualized in **Fig 7b**) that reconciles our observed geochemical data, the $\delta^{34}S$ of this initial SO_4^{2-} must be -11‰ or lower. After a Rayleigh distillation process in which at least 93% of SO_4^{2-} is converted to H_2S (assuming a closed system), isotopically enriched SO_4^{2-} of $\delta^{34}S \geq 45‰$ reaches the water column of the lake. Sulfide produced in this hydrothermal process either precipitates as pyrite within suevite or is volatilized out of the system. Water column SO_4^{2-} is then incorporated into CAS (white arrow), as well as reduced and incorporated into lacustrine CRS and kerogen (green arrow), with little to no additional fractionation (indicated by the data in **Figures 2, 3, and 4**). Approximate basin structure, lithology, and horizontal scale were adapted from Stöffler *et al.* (2013). Thin black lines indicating lacustrine sedimentary layering are aesthetic and do not represent geologic data. Paleolacustrine sediment thickness from this lake stage (*i.e.*, when $\delta^{34}S_{CRS} = 45.1‰$) is magnified three-fold (see left margin) with respect to the underlying suevite layer; thickness data are from the FBN 73 core only. For a detailed analysis of changes in the vertical extent of Ries crater sediments through time, see Arp *et al.* (2021).

References

Abramov O and Kring DA (2005) Impact-Induced Hydrothermal Activity on Early Mars. *J Geophys Res* 110(E12):E12S09; doi: 10.1029/2005JE002453.

Abramov O and Kring DA (2007) Numerical Modeling of Impact-Induced Hydrothermal Activity at the Chicxulub Crater. *Meteorit Planet Sci* 42(1):93–112; doi: 10.1111/j.1945-5100.2007.tb00220.x.

Arp G (1995) Lacustrine Bioherms, Spring Mounds, and Marginal Carbonates of the Ries-impact-crater (Miocene, southern Germany). *Facies* 33(1):35-89; doi: 10.1007/BF02537444.

Arp G (2006) Sediments of the Ries Crater Lake (Miocene, Southern Germany). *Schriftenreihe der deutschen Gesellschaft für Geowissenschaften* 45:213–236.Arp G, Bielert F, Hoffmann VE, *et al.* (2005) Palaeoenvironmental Significance of Lacustrine Stromatolites of the Arnstadt Formation ("Steinmergelkeuper", Upper Triassic, N-Germany). *Facies* 51(1–4):419–441; doi: 10.1007/s10347-005-0063-8.

Arp G, Blumenberg M, Hansen BT, *et al.* (2013a) Chemical and Ecological Evolution of the Miocene Ries Impact Crater Lake, Germany: A Reinterpretation Based on the Enkingen (SUBO 18) Drill Core. *Geol Soc Am Bull* 125(7–8):1125–1145; doi: 10.1130/B30731.1.

Arp G, Dunkl I, Jung D, *et al.* (2021a) A Volcanic Ash Layer in the Nördlinger Ries Impact Structure (Miocene, Germany): Indication of Crater Fill Geometry and Origins of Long-Term Crater Floor Sagging. *J Geophys Res Planets* 126(4); doi: 10.1029/2020JE006764.

Arp G, Gropengießer S, Schulbert C, *et al.* (2021b) Biostratigraphy and sequence stratigraphy of the Toarcian Ludwigskanal section (Franconian Alb, Southern Germany). *Zitteliana* 95:57-94; doi: 10.3897/zitteliana.95.56222.

Arp G, Hansen BT, Pack A, *et al.* (2017) The Soda Lake—Mesosaline Halite Lake Transition in the Ries Impact Crater Basin (Drilling Löpsingen 2012, Miocene, Southern Germany). *Facies* 63(1):1; doi: 10.1007/s10347-016-0483-7.

Arp G, Kolepka C, Simon K, *et al.* (2013b) New Evidence for Persistent Impact-Generated Hydrothermal Activity in the Miocene Ries Impact Structure, Germany. *Meteorit Planet Sci* 48(12):2491–2516; doi: 10.1111/maps.12235.

Artemieva NA, Wünnemann K, Krien F, *et al.* (2013) Ries Crater and Suevite Revisited-Observations and Modeling Part II: Modeling. *Meteorit Planet Sci* 48(4):590–627; doi: 10.1111/maps.12085.

Barakat AO, Baumgart S, Brocks P, *et al.* (2012) Alkylated Phenol Series in Lacustrine Black Shales from the Nördlinger Ries, Southern Germany. *J Mass Spectrom* 47(8):987–994; doi: 10.1002/jms.3049.

Barakat AO, Peakman TM and Rullkötter J (1994) Isolation and Structural Characterization of 10-Oxo-Octadecanoic Acid in Some Lacustrine Sediments from the Nördlinger Ries (Southern Germany). *Org Geochem* 21(8–9):841–847; doi: 10.1016/0146-6380(94)90043-4.

Barakat AO and Rullkötter J (1995) Extractable and Bound Fatty Acids in Core Sediments from the Nördlinger Ries, Southern Germany. *Fuel* 74(3):416–425; doi: 10.1016/0016-2361(95)93476-T.

Barakat AO and Rullkötter J (1997) A Comparative Study of Molecular Paleosalinity Indicators: Chromans, Tocopherols and C20 Isoprenoid Thiophenes in Miocene Lake Sediments (Nördlinger Ries, Southern Germany). *Aquat Geochem* 3(2):169–190; doi: 10.1023/A:1009645510876.

Barakat AO, Scholz-Böttcher BM and Rullkötter J (2013) Lipids in a Sulfur-Rich Lacustrine Sediment from the Nördlinger Ries (Southern Germany) with a Focus on Free and Bound Sterols. *Geochem J* 47(4):397–407; doi: 10.2343/geochemj.2.0258.

Barkan Y, Paris G, Webb SM, *et al.* (2020) Sulfur isotope fractionation between aqueous and carbonate-associated sulfate in abiotic calcite and aragonite. *Geochim Cosmochim Acta* 280:317–339; doi: 10.1016/j.gca.2020.03.022.

Barlow NG (2005) A Review of Martian Impact Crater Ejecta Structures and Their Implications for Target Properties. In: *Large Meteorite Impacts III Geological Society of America* pp. 433–442; doi: 10.1130/0-8137-2384-1.433.

Baune C and Böttcher ME (2010) Experimental Investigation of Sulphur Isotope Partitioning during Outgassing of Hydrogen Sulphide from Diluted Aqueous Solutions and Seawater. *Isotopes Environ and Health Stud* 46(4):444–453; doi: 10.1080/10256016.2010.536230.

Berger JA, Schmidt ME, Gellert R, *et al.* (2017) Zinc and Germanium in the Sedimentary Rocks of Gale Crater on Mars Indicate Hydrothermal Enrichment Followed by Diagenetic Fractionation. *J Geophys Res Planets* 122(8):1747–1772; doi: 10.1002/2017JE005290.

Berner ZA, Puchelt H, Nöltner T, *et al.* (2013) Pyrite Geochemistry in the Toarcian Posidonia Shale of South-West Germany: Evidence for Contrasting Trace-Element Patterns of Diagenetic and Syngenetic Pyrites. *Sedimentology* 60(2):548–573; doi: 10.1111/j.1365-3091.2012.01350.x.

Böttcher ME, Brumsack H-J and de Lange GJ (1998) Sulfate Reduction and Related Stable Isotope (^{34}S, ^{18}O) Variations in Interstitial Waters from the Eastern Mediterranean. In: *Proceedings of the Ocean Drilling Program, 160 Scientific Results Ocean Drilling Program*; doi: 10.2973/odp.proc.sr.160.002.1998.

Böttcher ME and Schnetger B (2004) Direct Measurement of the Content and Isotopic Composition of Sulfur in Black Shales by Means of Combustion-Isotope-Ratio-Monitoring Mass Spectrometry (C-IrmMS). In: (P de Groot, ed.) *Handbook of Stable Isotope Analytical Techniques, Part I,* pp. 597–603; doi: 10.1016/B978-044451114-0/50029-6.

Böttcher ME, Sievert SM and Kuever J (1999) Fractionation of Sulfur Isotopes during Dissimilatory Reduction of Sulfate by a Thermophilic Gram-Negative Bacterium at 60 °C. *Arch Microbiol* 172(2):125–128; doi: 10.1007/s002030050749.

Brand WA and Coplen TB (2012) Stable Isotope Deltas: Tiny, yet Robust Signatures in Nature. *Isot Environ Health Stud* 48(3):393–409; doi: 10.1080/10256016.2012.666977.

Brunner B, Bernasconi SM, Kleikemper J, *et al.* (2005) A Model for Oxygen and Sulfur Isotope Fractionation in Sulfate during Bacterial Sulfate Reduction Processes. *Geochim Cosmochim Acta* 69(20):4773–4785; doi: 10.1016/j.gca.2005.04.017.

Butler IB, Böttcher ME, Rickard D, *et al.* (2004) Sulfur isotope partitioning during experimental formation of pyrite via the polysulfide and hydrogen sulphide pathways: Implications for the interpretation of sedimentary and hydrothermal pyrite isotope records. *Earth Planet Sci Lett* 228(3-4):495-509; doi: 10.1016/j.epsl.2004.10.005.

Cai C, Li H, Li K, *et al.* (2022) Thermochemical sulfate reduction in sedimentary basins and beyond: A review. *Chem Geol* 121018; doi: 10.1016/j.chemgeo.2022.121018.

Canfield DE (2001) Biogeochemistry of Sulfur Isotopes. *Rev Mineral Geochem* 43; doi: 10.2138/gsrmg.43.1.607.

Canfield DE, Farquhar J and Zerkle AL (2010) High Isotope Fractionations during Sulfate Reduction in a Low-Sulfate Euxinic Ocean Analog. *Geology* 38(5); doi: 10.1130/G30723.1.

Canfield DE, Habicht KS and Thamdrup B (2000) The Archean Sulfur Cycle and the Early History of Atmospheric Oxygen. *Science* 288(5466):658–661; doi: 10.1126/science.288.5466.658.

Canfield DE, Raiswell R, Westrich JT, *et al.* (1986) The Use of Chromium Reduction in the Analysis of Reduced Inorganic Sulfur in Sediments and Shales. *Chem Geol* 54(1–2):149–155; doi: 10.1016/0009-2541(86)90078-1.

Caudill C, Osinski GR, Greenberger RN, *et al.* (2021) Origin of the Degassing Pipes at the Ries Impact Structure and Implications for Impact-induced Alteration on Mars and Other Planetary Bodies. *Meteorit Planet Sci* 56(2):404–422; doi: 10.1111/maps.13600.

Clark BC, Baird AK, Weldon RJ, *et al.* (1982) Chemical Composition of Martian Fines. *J Geophys Res* 87(B12):10059; doi: 10.1029/JB087iB12p10059.

Cockell CS, Osinski G, Sapers H, *et al.* (2020) Microbial Life in Impact Craters. *Curr Issues Mol Biol* 38; doi: 10.21775/cimb.038.075.

Collins A (1975) *Geochemistry of Oilfield Waters*. Elsevier.

Crowe SA, Paris G, Katsev S, *et al.* (2014) Sulfate Was a Trace Constituent of Archean Seawater. *Science* 346(6210):735–739; doi: 10.1126/science.1258966.

Davidson MM, Bisher ME, Pratt LM, *et al.* (2009) Sulfur Isotope Enrichment during Maintenance Metabolism in the Thermophilic Sulfate-Reducing Bacterium Desulfotomaculum Putei. *Appl Environ Microbiol* 75(17):5621–5630; doi: 10.1128/AEM.02948-08.

Deamer D, Damer B and Kompanichenko V. (2019). Hydrothermal Chemistry and the Origin of Cellular Life. *Astrobiology* 19(12):1523-1537. doi: 10.1089/ast.2018.1979.

Ding T, Valkiers S, Kipphardt H, *et al.* (2001) Calibrated Sulfur Isotope Abundance Ratios of Three IAEA Sulfur Isotope Reference Materials and V-CDT with a Reassessment of the Atomic Weight of Sulfur. *Geochim Cosmochim Acta* 65(15):2433–2437; doi: 10.1016/S0016-7037(01)00611-1.

Di Vincenzo G (2022) High precision multi-collector $^{40}Ar/^{39}Ar$ dating of moldavites (Central European tektites) reconciles geochrological and paleomagnetic data. *Chem Geol* 608:121026; doi: 10.1016/j.chemgeo.2022.121026.

Eigenbrode JL, Summons RE, Steele A, *et al.* (2018) Organic Matter Preserved in 3-Billion-Year-Old Mudstones at Gale Crater, Mars. *Science* 360(6393):1096–1101; doi: 10.1126/science.aas9185.

Elsgaard L, Isaksen MF, Jørgensen BB, *et al.* (1994) Microbial Sulfate Reduction in Deep-Sea Sediments at the Guaymas Basin Hydrothermal Vent Area: Influence of Temperature and Substrates. *Geochim Cosmochim Acta* 58(16):3335–3343; doi: 10.1016/0016-7037(94)90089-2.

Eldridge DL, Guo W and Farquhar J (2016) Theoretical Estimates of Equilibrium Sulfur Isotope Effects in Aqueous Sulfur Systems: Highlighting the Role of Isomers in the Sulfite and Sulfoxylate Systems. *Geochim Cosmochim Acta* 195:171–200; doi: 10.1016/j.gca.2016.09.021.

Farmer JD (2000) Hydrothermal Systems: Doorways to Early Biosphere Evolution. *GSA Today* 10(7).

Fichtner V, Strauss H, Immenhauser A, *et al.* (2017) Diagenesis of Carbonate Associated Sulfate. *Chem Geol* 463:61–75; doi: 10.1016/j.chemgeo.2017.05.008.

Förstner VU (1977) Geochemische Untersuchungen an den Sedimenten des Ries-Sees (Forschungsbohrung Nördlingen 1973). *Geol Bavarica* 75:13–19.

Franz HB, King PL and Gaillard F (2019) Sulfur on Mars from the Atmosphere to the Core. In: *Volatiles in the Martian Crust* doi: 10.1016/B978-0-12-804191-8.00006-4.

Franz HB, McAdam AC, Ming DW, *et al.* (2017) Large Sulfur Isotope Fractionations in Martian Sediments at Gale Crater. *Nat Geosci* 10(9):658–662; doi: 10.1038/ngeo3002.

Fry B, Gest H and Hayes JM (1986) Sulfur Isotope Effects Associated with Protonation of HS^- and Volatilization of H_2S. *Chem Geol* 58(3):253–258; doi: 10.1016/0168-9622(86)90014-X.

Füchtbauer H, von der Brelie G, Dehm R, *et al.* (1977) Tertiary lake sediments of the Ries, research borehole Nördlingen 1973 - a summary. *Geol Bavarica* 75:13–19.

Gill BC, Lyons TW and Frank TD (2008) Behavior of Carbonate-Associated Sulfate during Meteoric Diagenesis and Implications for the Sulfur Isotope Paleoproxy. *Geochim Cosmochim Acta* 72(19):4699–4711; doi: 10.1016/j.gca.2008.07.001.

Goldfarb RJ, Newberry RJ, Pickthorn WJ, *et al.* (1991) Oxygen, hydrogen, and sulfur isotope studies in the Juneau gold belt, southeastern Alaska; constraints on the origin of hydrothermal fluids. *Econ Geol* 86(1):66–80; doi: 10.2113/gsecongeo.86.1.66.

Goudge TA, Mustard JF, Head JW, *et al.* (2015) Assessing the Mineralogy of the Watershed and Fan Deposits of the Jezero Crater Paleolake System, Mars. *J Geophys Res Planets* 120(4); doi: 10.1002/2014JE004782.

Graup G (1999) Carbonate-Silicate Liquid Immiscibility upon Impact Melting: Ries Crater, Germany. *Meteorit Planet Sci* 34(3):425–438; doi: 10.1111/j.1945-5100.1999.tb01351.x.

Grotzinger JP, Gupta S, Malin MC, *et al.* (2015) Deposition, Exhumation, and Paleoclimate of an Ancient Lake Deposit, Gale Crater, Mars. *Science* 350(6257); doi: 10.1126/science.aac7575.

Habicht KS, Gade M, Thamdrup B, *et al.* (2002) Calibration of Sulfate Levels in the Archean Ocean. *Science* 298(5602):2372–2374; doi: 10.1126/science.1078265.

Habicht KS, Salling L, Thamdrup B, *et al.* (2005) Effect of Low Sulfate Concentrations on Lactate Oxidation and Isotope Fractionation during Sulfate Reduction by *Archaeoglobus Fulgidus* Strain Z. *Appl Environ Microbiol* 71(7):3770–3777; doi: 10.1128/AEM.71.7.3770-3777.2005.

Hamilton-Brehm SD, Gibson RA, Green SJ, *et al.* (2013) *Thermodesulfobacterium Geofontis* Sp. Nov., a Hyperthermophilic, Sulfate-Reducing Bacterium Isolated from Obsidian Pool, Yellowstone National Park. *Extremophiles* 17(2):251–263; doi: 10.1007/s00792-013-0512-1.

Harrison AG and Thode HG (1958) Mechanism of the Bacterial Reduction of Sulphate from Isotope Fractionation Studies. *Trans Faraday Soc* 54:84; doi: 10.1039/tf9585400084.

Hartmann M and Nielsen H (2012) $\delta^{34}S$ Values in Recent Sea Sediments and Their Significance Using Several Sediment Profiles from the Western Baltic Sea. *Isot Environ Health Stud* 48(1):7–32; doi: 10.1080/10256016.2012.660528.

Hays LE, Graham HV, des Marais DJ, *et al.* (2017) Biosignature Preservation and Detection in Mars Analog Environments. *Astrobiology* 17(4); doi: 10.1089/ast.2016.1627.

Hendrix AR, Hurford TA, Barge LM, *et al.* (2019) The NASA Roadmap to Ocean Worlds. *Astrobiology* 19(1):1-27; doi: 10.1089/ast.2018.1955.

Hoefs J. (2021) *Stable Isotope Geochemistry*. *3rd ed.* Springer International Publishing; doi: 10.1007/978-3-030-77692-3.

Hörz F, Ostertag R and Rainey DA (1983) Bunte Breccia of the Ries: Continuous Deposits of Large Impact Craters. *Rev Geophys* 21(8):1667; doi: 10.1029/RG021i008p01667.

Hofmann P, Leythaeuser D and Schwark L (2001) Organic Matter from the Bunte Breccia of the Ries Crater, Southern Germany: Investigating Possible Thermal Effects of the Impact. *Planet Space Sci* 49(8):845–851; doi: 10.1016/S0032-0633(01)00034-4.

Ivanov BA (2004) Heating of the Lithosphere during Meteorite Cratering. *Sol Syst Res* 38(4):266–279; doi: 10.1023/B:SOLS.0000037462.56729.ba.

Jankowski B (1977) Die Postimpakt-Sedimente in der Forschungsbohrung Nördlingen 1973. *Geol Bavarica* 75:21–36.
Jørgensen BB, Isaksen MF and Jannasch HW (1992) Bacterial Sulfate Reduction Above 100°C in Deep-Sea Hydrothermal Vent Sediments. *Science* 258(5089):1756–1757; doi: 10.1126/science.258.5089.1756.
Kacar B, Garcia AK and Anbar AD (2021) Evolutionary History of Bioessential Elements Can Guide the Search for Life in the Universe. *ChemBioChem* 114-119; doi: 10.1002/cbic.202000500
Kaplan IR and Rittenberg SC (1964) Microbiological Fractionation of Sulphur Isotopes. *J Gen Microbiol* 34(2):195–212; doi: 10.1099/00221287-34-2-195.
Kenkmann T, Schönian F. Ries and Chicxulub: Impact craters on Earth provide insights for Martian ejecta blankets. Meteorit. Planet. Sci 2006;41(10):1587-1603; doi: 10.1111/j.1945-5100.2006.tb00437.x
King PL and McLennan SM (2010) Sulfur on Mars. *Elements* 6(2); doi: 10.2113/gselements.6.2.107.
Kirsimäe K and Osinski GR (2012) Impact-Induced Hydrothermal Activity. In: *Impact Cratering* (Osinski GR and Pierazzo E eds) pp. 76–89; doi: 10.1002/9781118447307.ch6.
Kring DA (2000) Impact Events and Their Effect on the Origin, Evolution, and Distribution of Life. *GSA Today* 10(8).
Kring DA, Whitehouse MJ and Schmieder M (2021) Microbial Sulfur Isotope Fractionation in the Chicxulub Hydrothermal System. *Astrobiology* 21(1):103–114; doi: 10.1089/ast.2020.2286.
Kutuzov I, Rosenberg YO, Bishop A, *et al.* (2020) The Origin of Organic Sulphur Compounds and Their Impact on the Paleoenvironmental Record. *In: (Wilkes H, ed.) Hydrocarbons, Oils and Lipids: Diversity, Origin, Chemistry and Fate, Handbook of Hydrocarbon and Lipid Microbiology*; doi: 10.1007/978-3-319-90569-3_1.
Liaghati T, Cox ME and Preda M (2005) Distribution of Fe in Waters and Bottom Sediments of a Small Estuarine Catchment, Pumicestone Region, Southeast Queensland, Australia. *Sci Tot Env* 336(1–3):243–254; doi: 10.1016/j.scitotenv.2004.05.028.
Léveillé R (2010) A Half-Century of Terrestrial Analog Studies: From Craters on the Moon to Searching for Life on Mars. *Planet Space Sci* 58(4); doi: 10.1016/j.pss.2009.04.001.
Lorand J, Labidi J, Rollion-Bard C, *et al.* (2020) The Sulfur Budget and Sulfur Isotopic Composition of Martian Regolith Breccia NWA 7533. *Meteorit Planet Sci* 55(9):2097–2116; doi: 10.1111/maps.13564.
Lyons TW and Gill BC (2016) Ancient Sulfur Cycling and Oxygenation of the Early Biosphere. *Elements* 6(2):93–99; doi: 10.2113/gselements.6.2.93.
Ma Q, Ellis GS, Amrani A, Zhang T and Tang Y (2008) Theoretical Study on the Reactivity of Sulfate Species with Hydrocarbons. *Geochim Cosmochim Acta* 72(18):4565-4576; doi: 10.1016/j.gca.2008.05.061.
Machel HG (1987) Some Aspects of Diagenetic Sulphate-hydrocarbon Redox Reactions. *Geol Soc Spec Publ* 36(1):15-28; doi: https://doi.org/10.1144/GSL.SP.1987.036.01.03.
Machel HG (2001) Bacterial and Thermochemical Sulfate Reduction in Diagenetic Settings — Old and New Insights. *Sediment Geol* 140(1–2):143–175; doi: 10.1016/S0037-0738(00)00176-7.
Machel HG, Krouse HR and Sassen R (1995) Products and Distinguishing Criteria of Bacterial and Thermochemical Sulfate Reduction. *Appl Geochem* 10(4):373–389; doi: 10.1016/0883-2927(95)00008-8.

Mangold N, Gupta S, Gasnault O, *et al.* (2021) Perseverance Rover Reveals an Ancient Delta-Lake System and Flood Deposits at Jezero Crater, Mars. *Science* 374(6568); doi: 10.1126/science.abl4051.

Marini L, Moretti R and Accornero M (2011) Sulfur Isotopes in Magmatic-Hydrothermal Systems, Melts, and Magmas. *Rev Mineral Geochem* 73(1):423–492; doi: 10.2138/rmg.2011.73.14.

McLennan SM, Anderson RB, Bell JF, *et al.* (2014) Elemental Geochemistry of Sedimentary Rocks at Yellowknife Bay, Gale Crater, Mars. *Science* 343(6169); doi: 10.1126/science.1244734.

Meshoulam A, Ellis GS, Said Ahmad W, *et al.* (2016) Study of Thermochemical Sulfate Reduction Mechanism Using Compound Specific Sulfur Isotope Analysis. *Geochim Cosmochim Acta* 188:73–92; doi: 10.1016/j.gca.2016.05.026.

Mitchell K, Heyer A, Canfield DE, *et al.* (2009) Temperature Effect on the Sulfur Isotope Fractionation during Sulfate Reduction by Two Strains of the Hyperthermophilic *Archaeoglobus Fulgidus*. *Environ Microbiol* 11(12):2998–3006; doi: 10.1111/j.1462-2920.2009.02002.x.

Montano D, Gasparrini M, Gerdes A, *et al.* (2021) In-Situ U-Pb Dating of Ries Crater Lacustrine Carbonates (Miocene, South-West Germany): Implications for Continental Carbonate Chronostratigraphy. Earth and Planetary Science Letters 568:117011; doi: 10.1016/j.epsl.2021.117011.

Muttik N, Kirsimäe K, Newsom HE, *et al.* (2011) Boron Isotope Composition of Secondary Smectite in Suevites at the Ries Crater, Germany: Boron Fractionation in Weathering and Hydrothermal Processes. *Earth Planet Sci Lett* 310(3–4):244–251; doi: 10.1016/j.epsl.2011.08.028.

Muttik N, Kirsimäe K and Vennemann TW (2010) Stable Isotope Composition of Smectite in Suevites at the Ries Crater, Germany: Implications for Hydrous Alteration of Impactites. *Earth Planet Sci Lett* 299(1–2):190–195; doi: 10.1016/j.epsl.2010.08.034.

Newsom HE, Graup G, Iseri DA, *et al.* (1990) The Formation of the Ries Crater, West Germany; Evidence of Atmospheric Interactions during a Larger Cratering Event. In: *Global Catastrophes in Earth History; An Interdisciplinary Conference on Impacts, Volcanism, and Mass Mortality* pp. 195–206; doi: 10.1130/SPE247-p195.

Newsom HE, Graup G, Sewards T, *et al.* (1986) Fluidization and Hydrothermal Alteration of the Suevite Deposit at the Ries Crater, West Germany, and Implications for Mars. *J Geophys Res* 91(B13):E239; doi: 10.1029/JB091iB13p0E239.

Nielsen H (1985) Sulfur-Isotope Ratios in Strata-Bound Mineralizations in Central Europe. *Geol Jb* D 70:225-262.Nielsen H, Pilot J, Grinenko LN, *et al.* (1991) Lithospheric Sources of Sulphur, In: *Stable Isotopes: Natural and Anthropogenic Sulphur in the Environment* (Krouse HR and Grinenko VA, eds.) SCOPE-43: pp. 65–132.

Nozaki T, Nagase T, Ushikubo T, *et al.* (2020) Microbial Sulfate Reduction Plays an Important Role at the Initial Stage of Subseafloor Sulfide Mineralization. *Geology* 49(2):222-227; doi: 10.1130/G47943.1.

Ohfuji H and Rickard D (2005) Experimental Syntheses of Framboids—a Review. *Earth-Sci Rev* 71(3–4):147–170; doi: 10.1016/j.earscirev.2005.02.001.

Ohmoto H and Goldhaber MB (1997) Sulfur and Carbon Isotopes. *Geochemistry of Hydrothermal Ore Deposits. 3rd ed.*

Orr WL (1974) Changes in Sulfur Content and Isotopic Ratios of Sulfur during Petroleum Maturation—Study of Big Horn Basin Paleozoic Oils. *AAPG bulletin* 58(11):2295-2318; doi:

10.1306/83D91B9B-16C7-11D7-8645000102C1865D.Osinski GR (2005) Hydrothermal Activity Associated with the Ries Impact Event, Germany. *Geofluids* 5(3):202–220; doi: 10.1111/j.1468-8123.2005.00119.x.

Osinski GR, Cockell CS, Pontefract A, *et al.* (2020) The Role of Meteorite Impacts in the Origin of Life. *Astrobiology* 20(9):1121–1149; doi: 10.1089/ast.2019.2203.

Osinski GR, Grieve RAF, Chanou A, *et al.* (2016) The "Suevite" Conundrum, Part 1: The Ries Suevite and Sudbury Onaping Formation Compared. *Meteorit Planet Sci* 51(12):2316–2333; doi: 10.1111/maps.12728.

Osinski GR, Grieve RAF and Spray JG (2004) The Nature of the Groundmass of Surficial Suevite from the Ries Impact Structure, Germany, and Constraints on Its Origin. *Meteorit Planet Sci* 39(10):1655–1683; doi: 10.1111/j.1945-5100.2004.tb00065.x.

Osinski GR, Tornabene LL, Banerjee NR, *et al.* (2013) Impact-Generated Hydrothermal Systems on Earth and Mars. *Icarus* 224(2); doi: 10.1016/j.icarus.2012.08.030.

Pache M, Reitner J and Arp G (2001) Geochemical Evidence for the Formation of a Large Miocene "Travertine" Mound at a Sublacustrine Spring in a Soda Lake (Wallerstein Castle Rock, Nördlinger Ries, Germany). *Facies* 45(1):211–230; doi: 10.1007/BF02668114.

Parnell J, Boyce A, Thackrey S, *et al.* (2010) Sulfur Isotope Signatures for Rapid Colonization of an Impact Crater by Thermophilic Microbes. *Geology* 38(3):271–274; doi: 10.1130/G30615.1.

Passier HF, Middelburg JJ, de Lange GJ, *et al.* (1999) Modes of Sapropel Formation in the Eastern Mediterranean: Some Constraints Based on Pyrite Properties. *Mar Geol* 153(1–4):199–219; doi: 10.1016/S0025-3227(98)00081-4.

Pohl J, Poschlod K, Reimold WU, *et al.* (2010) Ries Crater, Germany: The Enkingen Magnetic Anomaly and Associated Drill Core SUBO 18. In: *Large Meteorite Impacts and Planetary Evolution IV*; doi: 10.1130/2010.2465(10).

Pohl J, Stöffler D, Gall H, *et al.* (1977) The Ries Impact Crater. In: *Impact and Explosion Cratering* (Roddy D, Pepin R, and Merrill R. eds) pp. 343–404.

Rampe EB, Blake DF, Bristow TF, *et al.* (2020) Mineralogy and Geochemistry of Sedimentary Rocks and Eolian Sediments in Gale Crater, Mars: A Review after Six Earth Years of Exploration with Curiosity. *Geochemistry* 80(2):125605; doi: 10.1016/j.chemer.2020.125605.

Reese BK, Anderson MA and Amrhein C (2008) Hydrogen Sulfide Production and Volatilization in a Polymictic Eutrophic Saline Lake, Salton Sea, California. *Sci Total Environ* 406(1–2):205–218; doi: 10.1016/j.scitotenv.2008.07.021.

Reimold WU, Hansen BK, Jacob J, *et al.* (2012) Petrography of the Impact Breccias of the Enkingen (SUBO 18) Drill Core, Southern Ries Crater, Germany: New Estimate of Impact Melt Volume. *Geol Soc Am Bull* 124(1–2):104–132; doi: 10.1130/B30470.1.

Reimold WU, McDonald I, Schmitt R-T, *et al.* (2013) Geochemical Studies of the SUBO 18 (Enkingen) Drill Core and Other Impact Breccias from the Ries Crater, Germany. *Meteorit Planet Sci*; doi: 10.1111/maps.12175.

Rickard D. Geochemistry of Framboids (2021) In: *Framboids* pp. 169–190; doi: 10.1093/oso/9780190080112.003.0009.

Rullkötter J, Littke R and Schaefer RG (1990) Characterization of Organic Matter in Sulfur-Rich Lacustrine Sediments of Miocene Age (Nördlinger Ries, Southern Germany). In: *Geochemistry of Sulfur in Fossil Fuels* pp. 149–169; doi: 10.1021/bk-1990-0429.ch008.

Sakai H (1957) Fractionation of Sulphur Isotopes in Nature. *Geochim Cosmochim Acta* 12(1–2):150–169; doi: 10.1016/0016-7037(57)90025-X.

Sakai H (1968) Isotopic Properties of Sulfur Compounds in Hydrothermal Processes. *Geochem J* 2(1):29–49; doi: 10.2343/geochemj.2.29.

Sandford SA, Nuevo M, Bera PP, *et al.* (2020) Prebiotic Astrochemistry and the Formation of Molecules of Astrobiological Interest in Interstellar Clouds and Protostellar Disks. *Chem Rev* 120(11):4616–4659; doi: 10.1021/acs.chemrev.9b00560.

Sapers HM, Osinski GR, Flemming RL, *et al.* (2017) Evidence for a Spatially Extensive Hydrothermal System at the Ries Impact Structure, Germany. *Meteorit Planet Sci* 52(2):351–371; doi: 10.1111/maps.12796.

Schaefer B, Grice K, Coolen MJL, *et al.* (2020) Microbial life in the nascent Chicxulub crater. *Geology* 48(4):328-332; doi: 10.1130/G46799.1.

Schaefer B, Schwark L, Böttcher ME, *et al.* (2022) Paleoenvironmental evolution during the Early Eocene Climate Optimum in the Chicxulub impact crater. *Earth Planet Sci Lett* 589:117589; doi: 10.1016/j.epsl.2022.1175.

Schwenzer SP and Kring DA (2009) Impact-generated Hydrothermal Systems Capable of Forming Phyllosilicates on Noachian Mars. *Geology* 37(12):1091-1094; doi: 10.1130/G30340A.1.

Seal RR (2006) Sulfur Isotope Geochemistry of Sulfide Minerals. *Rev Mineral Geochem* 61(1):633–677; doi: 10.2138/rmg.2006.61.12.

Sharp Z (2017) *Principles of Stable Isotope Geochemistry. 2nd ed.*

Sim MS, Bosak T and Ono S (2011) Large Sulfur Isotope Fractionation Does Not Require Disproportionation. *Science* 333(6038); doi: 10.1126/science.1205103.

Sim MS, Sessions AL, Orphan VJ, *et al.* (2019) Precise Determination of Equilibrium Sulfur Isotope Effects during Volatilization and Deprotonation of Dissolved H_2S. *Geochim Cosmochim Acta* 248:242–251; doi: 10.1016/j.gca.2019.01.016.

Squyres SW, Grotzinger JP, Arvidson RE, *et al.* (2004) In Situ Evidence for an Ancient Aqueous Environment at Meridiani Planum, Mars. *Science* 306(5702):1709–1714; doi: 10.1126/science.1104559.

Stetter KO (1988) *Archaeoglobus Fulgidus* Gen. Nov., Sp. Nov.: A New Taxon of Extremely Thermophilic Archaebacteria. *Syst Appl Microbiol* 10(2):172–173; doi: 10.1016/S0723-2020(88)80032-8.

Stetter KO, Lauerer G, Thomm M, *et al.* (1987) Isolation of Extremely Thermophilic Sulfate Reducers: Evidence for a Novel Branch of Archaebacteria. *Science* 236(4803):822–824; doi: 10.1126/science.236.4803.822.

Stöffler D (1977) Research Drilling Nördlingen 1973: Polymict Breccias, Crater Basement, and Cratering Model of the Ries Impact Structure. *Geol Bavarica* (75):443–458.

Stöffler D, Artemieva NA, Wünnemann K, *et al.* (2013) Ries Crater and Suevite Revisited-Observations and Modeling Part I: Observations. *Meteorit Planet Sci* 48(4):515–589; doi: 10.1111/maps.12086.

Stüeken EE, Tino CJ, Arp G, *et al.* (2020) Nitrogen Isotope Ratios Trace High-pH Conditions in a Terrestrial Mars Analog Site. *Sci Adv* 6(9); doi: 10.1126/sciadv.aay3440.

Sturm S, Wulf G, Jung D, *et al.* (2013) The Ries Impact, a Double-Layer Rampart Crater on Earth. *Geology* 41(5):531–534; doi: 10.1130/G33934.1.

Surkov A, Böttcher ME and Kuever J. (2012) Sulphur Isotope Fractionation during the Reduction of Elemental Sulphur and Thiosulphate by Dethiosulfovibrio spp. *Isot Environ Health Stud* 48(1):65–75; doi: 10.1080/10256016.2011.626525.

Thode HG, Monster J and Dunford HB (1961) Sulphur Isotope Geochemistry. *Geochim Cosmochim Acta* 25(3):159–174; doi: 10.1016/0016-7037(61)90074-6.

Vaniman DT, Bish DL, Ming DW, *et al.* (2014) Mineralogy of a Mudstone at Yellowknife Bay, Gale Crater, Mars. *Science* 343(6169); doi: 10.1126/science.1243480.

Viola D, McEwen AS, Dundas CM, *et al.* (2017) Subsurface Volatile Content of Martian Double-Layer Ejecta (DLE) Craters. *Icarus* 284:325–343; doi: 10.1016/j.icarus.2016.11.031.

von Engelhardt W (1997) Suevite Breccia of the Ries Impact Crater, Germany: Petrography, Chemistry and Shock Metamorphism of Crystalline Rock Clasts. *Meteorit Planet Sci* 32(4):545–554; doi: 10.1111/j.1945-5100.1997.tb01299.x.

von Engelhardt W (1990) Distribution, Petrography and Shock Metamorphism of the Ejecta of the Ries Crater in Germany—a Review. *Tectonophysics* 171(1–4):259–273; doi: 10.1016/0040-1951(90)90104-G.

von Gehlen K and Nielsen H (1985) Sulfur Isotopes and the Formation of Stratabound Lead-Bearing Triassic Sandstones in Northeastem Bavaria. *Geol Jb* D 70:212-223.

Watanabe Y, Farquhar J and Ohmoto H (2009) Anomalous Fractionations of Sulfur Isotopes During Thermochemical Sulfate Reduction. *Science* 324(5925); doi: 10.1126/science.1169289.

Weber A and Jørgensen BB (2002) Bacterial Sulfate Reduction in Hydrothermal Sediments of the Guaymas Basin, Gulf of California, Mexico. Deep Sea Research Part I: Oceanographic Research Papers 49(5):827–841; doi: 10.1016/S0967-0637(01)00079-6.

Westrich JT and Berner RA (1984) The Role of Sedimentary Organic Matter in Bacterial Sulfate Reduction: The G Model Tested[1]. *Limnol Oceanogr* 29(2):236–249; doi: 10.4319/lo.1984.29.2.0236.

Winkler H (1972) Das Grundwasser Im Nördlinger Ries Unter Berücksichtigung Der Hydrologischen Und Hydrochemischen Beziehungen Zum Speichergestein. *Ludwig-Maximilians-Universität: München*.

Wolf M (1977) Kohlenpetrographische Untersuchungen der See-Sedimente der Forschungsbohrung Nördlingen 1973 und Vergleich mit anderen Untersuchungsergebnissen aus dem Ries. *Geol Bavarica* 75:127-138.

Wordsworth R, Knoll AH, Hurowitz J, *et al.* (2021) A Coupled Model of Episodic Warming, Oxidation and Geochemical Transitions on Early Mars. *Nat Geosci* 14(3):127–132; doi: 10.1038/s41561-021-00701-8.

Wortmann UG, Bernasconi SM and Böttcher ME (2001) Hypersulfidic Deep Biosphere Indicates Extreme Sulfur Isotope Fractionation during Single-Step Microbial Sulfate Reduction. *Geology* 29(7):647; doi: 10.1130/0091-7613(2001)029<0647:HDBIES>2.0.CO;2.

Yang S, Schulz H-M, Horsfield B, *et al.* (2020) Geological Alteration of Organic Macromolecules by Irradiation: Implication for Organic Matter Occurrence on Mars. *Geology* 48(7):713–717; doi: 10.1130/G47171.1.

Zhang T, Amrani A, Ellis GS, Ma Q and Tang Y (2008) Experimental Investigation on Thermochemical Sulfate Reduction by H_2S Initiation. *Geochim Cosmochim Acta* 72(14):3518-3530; doi: 10.1016/j.gca.2008.04.036.